WMO/IOC/UNEP/ICSU
GLOBAL CLIMATE OBSERVING SYSTEM (GCOS)

Doc. 5.4
(16.II.2011)

3rd GRUAN Implementation-Coordination Meeting (ICM-3)
Queenstown, New Zealand
28 February – 4 March 2011

Session 5

Site report: Tateno, Japan

(Submitted by Hakaru MIZUNO, Japan Meteorological Agency)

Summary and Purpose of Document

This document describes a comparison of the Meisei RS2-91-type radiosonde with the Vaisala RS92-SGPJ-type radiosonde carried out at Tateno in Japan from December 2009 to October 2010, and spatial variability for GPS derived precipitable water vapor to discuss collocation issue of observation.

PART I COMPARISON OF MEISEI RS2-91 with VAISALA RS92-SGPJ

1. Introduction

Figure 1 shows the Japan Meteorological Agency (JMA) upper-air observation network consisting of 16 radiosonde stations that observe temperature, humidity and wind at 00 UTC (09 LST) and 12 UTC (21 LST). JMA also makes observations at 06 UTC (15 LST) and 18 UTC (03 LST) if there is a typhoon within 300 km of the Japanese mainland. Six stations, including Tateno, are registered as GCOS Upper-air Network (GUAN) sites.

JMA used Meisei RS2-91 radiosondes with a radio-direction wind-finding system at all stations until March 2002, but started to replace them with GPS radiosondes from April 2002 to improve data acquisition and accuracy. Observations made using the Vaisala RS92-SGPJ-type GPS radiosonde were started in December 2009 at Tateno. In relation to the transition from the Meisei RS2-91-type radiosonde to the Vaisala RS92-SGPJ-type GPS radiosonde, JMA carried out a series of comparison launches of the Meisei RS2-91 with the Vaisala RS92-SGPJ at Tateno from December 2009 to October 2010. The purpose of this document is to describe the results of the comparison.

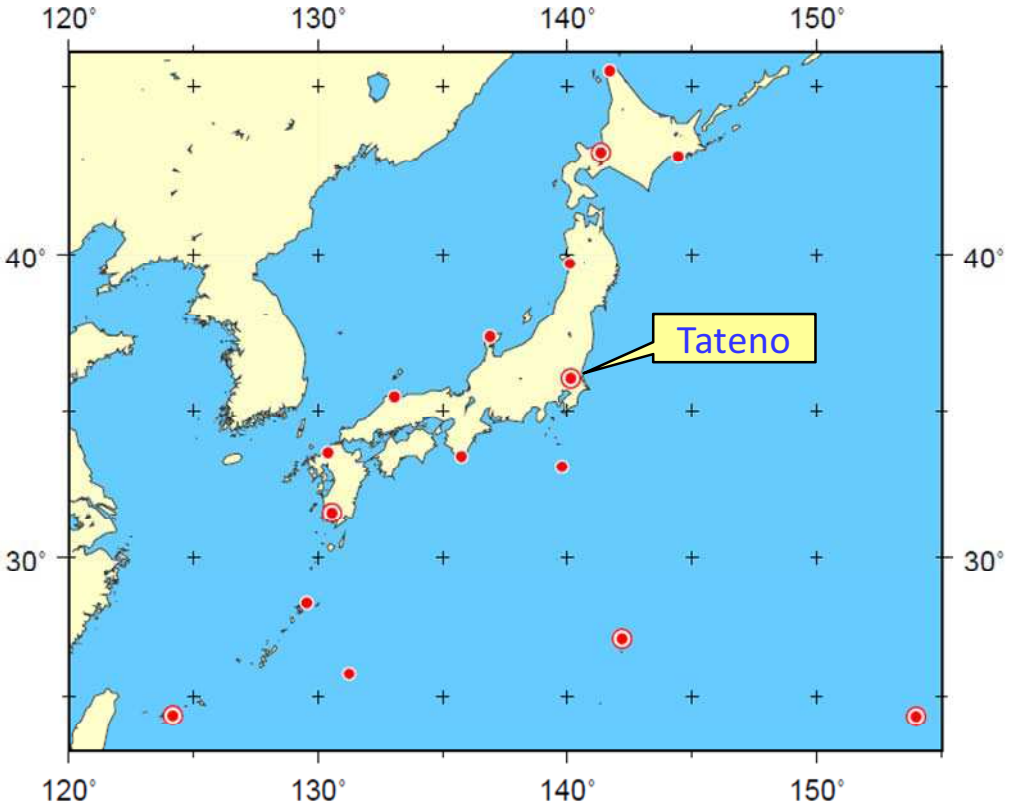

Figure 1. Radiosonde stations (solid circles) and GUAN stations (double solid circles) in the Japan Meteorological Agency (JMA) upper-air observation network.

2. Overview of the Meisei RS2-91 and the Vaisala RS92-SGPJ

Table 1 shows the specifications of the Meisei RS2-91 radiosonde (Meisei, 2010) and the Vaisala RS92-SGPJ radiosonde (Vaisala, 2010). The Meisei RS2-91 model was introduced into operational upper-air observation at Tateno in October 1992, and the Vaisala RS92-SGPJ was introduced in December 2009. The Meisei RS2-91 was used in WMO international radiosonde comparisons in 1993 in Japan (Yagi et al., 1996), as was the Vaisala RS92-SGP in 2005 at Mauritius (Nash et al., 2006). The RS92-SGPJ, a Japanese model of the RS92-SGP, has the same sensors as the RS92-SGP, a string or unwinder measuring 30 m in length and dry batteries.

The photo on the left of Figure 2 shows the temperature and humidity sensors of the Meisei RS2-91. The temperature sensor is a thermistor coated with vacuum-evaporated

aluminum to reduce the effects of infrared radiation. The humidity sensor is a capacitive thin polymer film element whose electrical capacity is monitored to ascertain ambient humidity. Both sensors are mounted on a sensor-holding plate, and the humidity sensor has a cap to prevent contamination from raindrops. The pressure sensor is a capacitive aneroid capsule whose electrical capacity is continuously monitored for changes caused by air pressure variations. Signals from each sensor are sampled every 4 seconds, frequency modulated and transmitted to the ground system, the JMA-91 system. The received signals are demodulated and converted to the values of pressure, temperature and humidity using pre-determined calibration data.

The photo on the right of Figure 2 shows the temperature and humidity sensors of the Vaisala RS92-SGPJ.The temperature sensor is a capacitive wire type that provides fast response and has a low need for radiation error correction. The humidity sensor is a thin polymer film capacitor with a heated twin sensor to prevent ice formation. The pressure sensor is a silicon model providing accurate pressure measurement.

Table 1. Radiosonde specifications

Type of radiosonde	Meisei RS2-91	Vaisala RS92-SGPJ
Temperature sensor		
Type	Rod thermistor	Capacitive wire
Size	10.0 mm ϕ 1.2 mm	
Time constant (6 m/s flow)	Surface 4.5 s	1,000 hPa ＜0.4 s
		100 hPa ＜ 1 s
		10hPa ≦2.5 s
Measurement range	-85˚C to +40˚C	-90˚C to +60˚C
Humidity sensor		
Type	Thin film capacitor	Thin film capacitor, heated twin sensor
Time constant (6 m/s flow)	Surface 4.5 s	1,000 hPa, 20˚C ＜0.5 s
		100 hPa, -40˚C ＜20 s
Measurement range	1 to 100%	0 to100%
Pressure sensor		
Type	Capacitive aneroid capsule	Silicon
Resolution	0.1 hPa	0.1 hPa
Measurement range	1,040 hPa – 5 hPa	1,080 hPa – 3 hPa

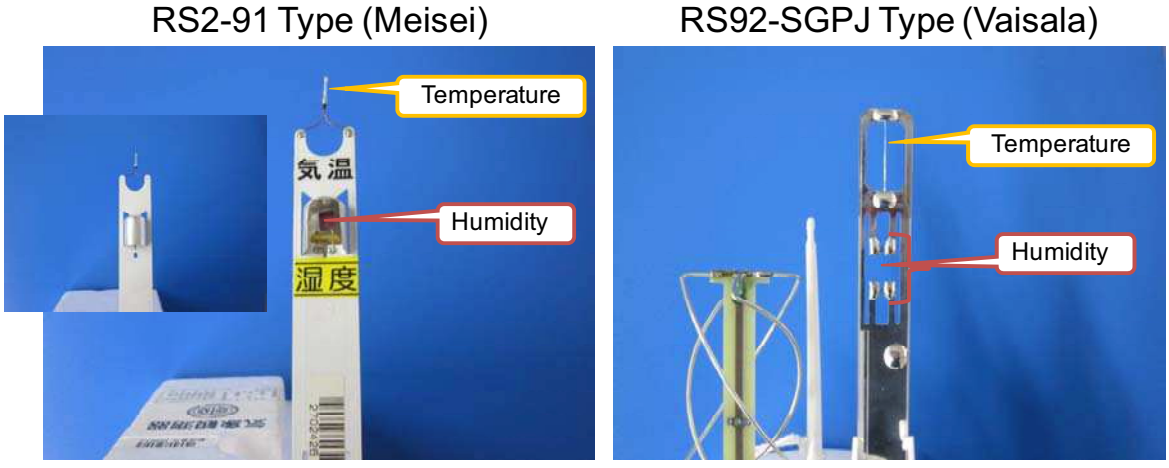

Figure 2. Temperature and humidity sensors of the Meisei RS2-91 and the Vaisala RS92-SGPJ.

Solar radiation correction for the Meisei RS2-91 was applied for air temperature measurements during the daytime, but no infrared radiation correction was applied either

during the day or at nighttime (JMA, 2004). The theoretical formula for temperature correction was developed from the heat balance model of a thermistor and its lead wire. The correction formula depends in a complex manner on such quantities as the heat transfer coefficient of the sensor and the solar radiation it receives. The average effect of shading by clouds is also taken into account. Figure 3 shows an example of solar radiation correction. In this case, the radiosonde is assumed to measure the temperature through the US Standard Atmosphere (1966) with a fixed rate of ascent of 6 m/s. It should be noted that solar radiation correction for the Meisei RS2-91 exceeds -1°C at altitudes above about 12 km and at solar elevation angle above 10 degrees.

Radiation correction for the temperature measurements of the Vaisala RS92-SGPJ is performed as shown in Table 2, which was provided by the manufacturer (Vaisala, 2005). It is also noted that radiation correction for the Vaisala RS92-SGPJ is smaller than that for the Meisei RS2-91.

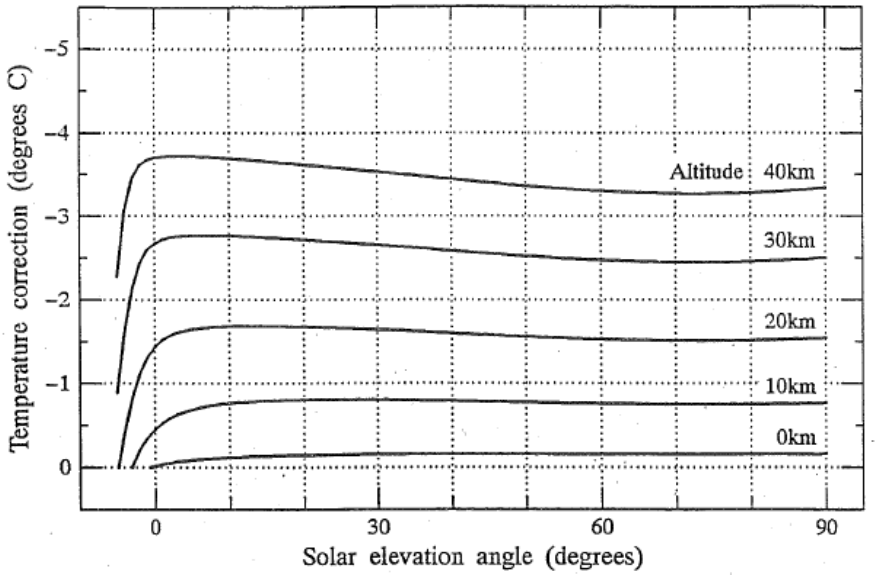

Figure 3. Example of solar radiation correction for the Meisei RS2-91 radiosonde (JMA, 2004).

Table 2. Radiation correction table for the Vaisala RS92-SGPJ (Vaisala, 2005).

Elevation angle [degrees]	Night	-5	-3	0	3	10	30	45	60	90
Sea Level	0 °C	0 °C	0 °C	0 °C	0 °C	0.01 °C	0.04 °C	0.06 °C	0.07 °C	0.1 °C
500 hPa	0 °C	0 °C	0 °C	0.04 °C	0.07 °C	0.11 °C	0.14 °C	0.14 °C	0.14 °C	0.14 °C
200 hPa	0 °C	0 °C	0.01 °C	0.11 °C	0.15 °C	0.19 °C	0.21 °C	0.2 °C	0.2 °C	0.21 °C
100 hPa	0 °C	0 °C	0.05 °C	0.18 °C	0.23 °C	0.27 °C	0.28 °C	0.27 °C	0.27 °C	0.27 °C
50 hPa	0 °C	0 °C	0.15 °C	0.28 °C	0.34 °C	0.38 °C	0.39 °C	0.37 °C	0.37 °C	0.37 °C
30 hPa	-0.01 °C	0 °C	0.21 °C	0.36 °C	0.42 °C	0.45 °C	0.45 °C	0.43 °C	0.43 °C	0.44 °C
20 hPa	-0.01 °C	0.11 °C	0.27 °C	0.44 °C	0.49 °C	0.53 °C	0.52 °C	0.5 °C	0.49 °C	0.5 °C
10 hPa	-0.01 °C	0.25 °C	0.35 °C	0.53 °C	0.58 °C	0.61 °C	0.6 °C	0.57 °C	0.57 °C	0.57 °C
5 hPa	-0.02 °C	0.35 °C	0.38 °C	0.58 °C	0.63 °C	0.65 °C	0.65 °C	0.62 °C	0.62 °C	0.63 °C

3. Field comparison

The purposes of performing a field comparison of the Meisei RS2-91 with the Vaisala RS92-SGPJ were to investigate systematic differences by looking at the radiosondes side by side in routine use and to utilize the comparison results for the improvement of instruments and observation methods.

3.1 Flight schedule

Table 3 shows the four intensive observation periods (IOPs) of the field comparison carried out at Tateno to encompass an entire annual cycle. As more dual soundings result in a more accurate mean bias between the two types of radiosondes (Peterson and Durre,

2004), 15 dual soundings were planned for each observation time of 00 UTC (09 LST) and 12 UTC (21 LST) for each IOP. The total number of successful dual soundings at these two times was 115. Several dual soundings with outliers were excluded when deriving a general trend for the mean and difference profiles between the two radiosondes. An outlier is defined as a value that differs by three times the standard deviation from the mean or more.

Official soundings were carried out twice a day at 00 UTC and 12 UTC, and these dual soundings were also considered official. The balloon was released 30 minutes before the observation time. Figure 4 shows annual variations in the solar elevation angle at 00 UTC (09 LST) for Tateno during the period from November 2009 to October 2010.

Table 3. Intensive observation periods in the field comparison of the Meisei RS2-91 with the Vaisala RS92-SGPJ.

IOP No.	Season	Period	Number of dual soundings		
			00 UTC (09 LST)	12 UTC (21 LST)	Total
1	Winter	3 Dec. 2009 to 15 Jan. 2010	14	15	29
2	Spring	1 Mar. 2010 to 19 Mar. 2010	15	15	30
3	Summer	24 May 2010 to 8 Jul. 2010	12	14	26
4	Autumn	27 Sep. 2010 to 26 Oct. 2010	15	15	30
1 – 4	**–**	**–**	**56**	**59**	**115**

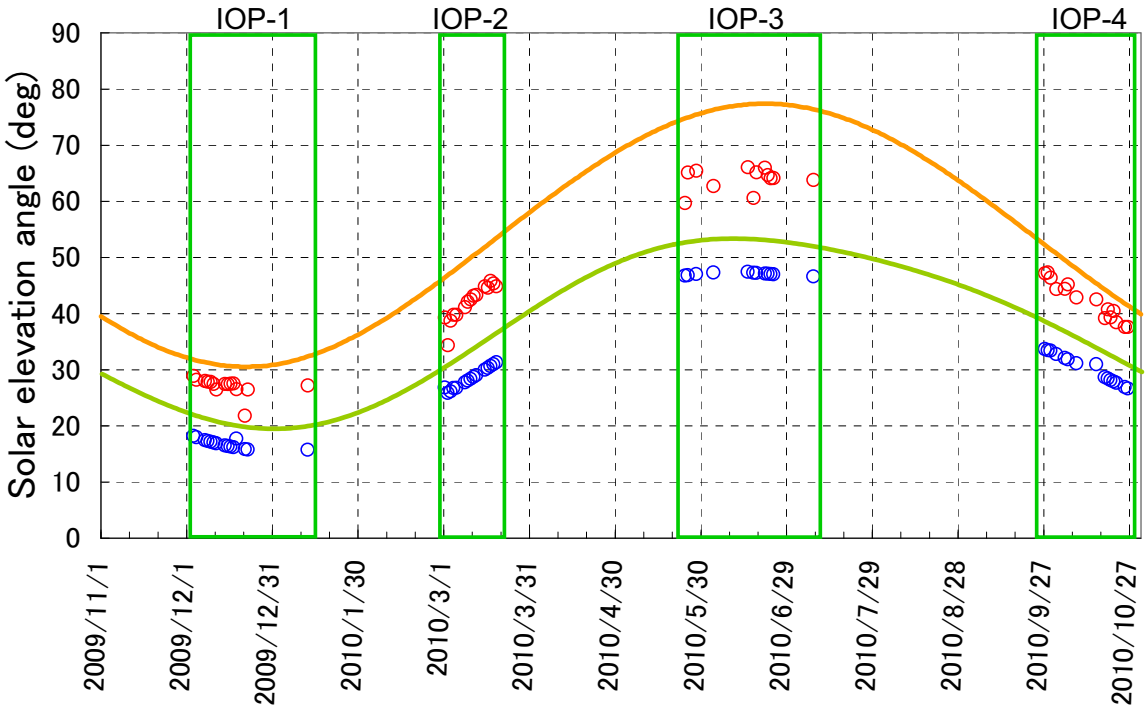

Figure 4. The green (▬) and orange (▬) lines show variations in the solar elevation angle at 00 UTC (09 LST) and the meridian passage time, respectively, in Tateno for the period from November 2009 to October 2010. The blue circles (○) indicate the solar elevation angle at the beginning of sounding, and the red circles (○) show that at the finishing time. The balloon was released 30 minutes before the observation time.

3.2 Flight configuration

Figure 5 indicates the flight configurations of dual soundings during IOP-1 and during IOP-2, IOP-3 and IOP-4. The configuration consists of a hydrogen-filled balloon, strings, a parachute and two radiosondes, the Meisei RS2-91 and the Vaisala RS92-SGPJ. The two radiosondes were hung below a piece of bamboo suspended beneath a 2,000-g balloon during IOP-1 and a 1,200-g balloon during IOP-2, IOP-3 and IOP-4. The distance between

the balloon and the radiosondes was about 60 m during IOP-1 and about 30 m during IOP-2, IOP-3 and IOP-4. The balloon's rate of ascent was typically planned to be 6 meters per second.

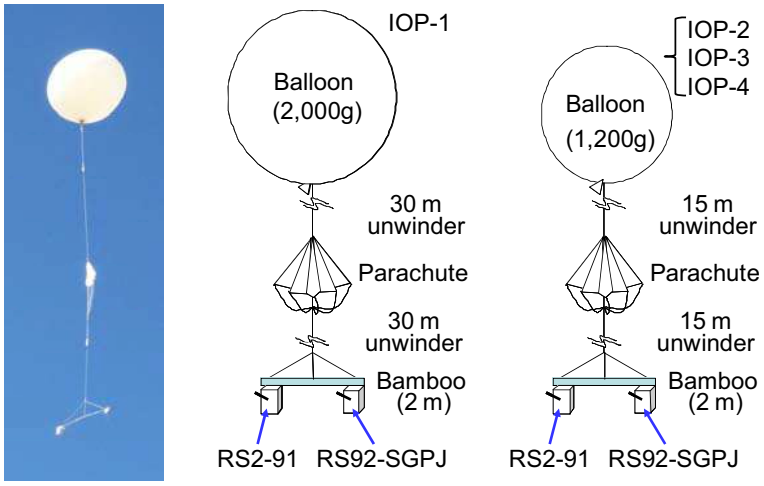

Figure 5. Flight configuration of dual soundings.

3.3 Pre-launch check

3.3.1 RS2-91 radiosonde

Pre-launch checks of the pressure, temperature and humidity sensors were made using a chamber in an observation room up to 30 minutes before the launch. The sensor readings were compared against the air pressure in the observation room (obtained from routine surface observation) and the temperature and humidity (obtained with a psychrometer) in the chamber. Sensors whose deviations from the reference values were within a specified limit (5 hPa, 0.5°C and 7%) were deemed fine for use in the observation. Pressure measurements were corrected during the ascent using the bias derived in this test.

3.3.2 RS92-SGPJ radiosonde

Pre-launch checks of the radiosonde sensors were made immediately before the launch with the Vaisala Ground Check Set GC25 and the Vaisala DigiCORA Sounding System MW31 (Software version 3.63). The pressure sensor was checked against a digital barometer that had been calibrated against a reference barometer, and the temperature sensor was checked against a reference Pt-100 sensor with traceability to the JMA temperature standard. The humidity sensor was checked using equipment whose humidity was kept near 0%. The results of these checks were entered into the GC25 ground equipment, and the measured pressure, temperature and humidity values were automatically corrected in data processing during the ascent.

3.4 Time adjustment procedure

As the measurements from the two radiosondes (the Meisei RS2-91 and the Vaisala RS92-SGPJ) were simultaneously obtained on the same balloon platform, the time elapsed since balloon release is the only common parameter relating to every instrument in any given observation. The time of launch for the RS2-91 radiosonde system was determined manually with a starting signal triggered by the operator, and automatically for the RS92-SGPJ system.

Figure 6 shows an example of the time adjustment procedure. To minimize the difference in the time elapsed between the radiosonde systems, an objective technique was used to adjust the times for all sets of radiosondes. As radiosonde measurements of temperature correspond more closely among the different types of radiosonde (da Silveira et al., 2006), temperature was used as the variable to drive the time offset adjustment. The time offset of the elapsed time for the RS2-91 radiosonde was estimated to maximize the correlation

coefficient (r_{xy}) between temperatures measured with two radiosondes as calculated from Equation (1).

$$r_{xy} = \frac{\sum_{i=1}^{n}(x_i - \bar{x})(y_i - \bar{y})}{\sqrt{\sum_{i=1}^{n}(x_i - \bar{x})^2}\sqrt{\sum_{i=1}^{n}(y_i - \bar{y})^2}} \qquad (1)$$

Where x_i is the temperature measured with the RS92-SGPJ at the time of observation, i; y_i is the temperature measured with the RS2-91; $\bar{x}$ is the mean temperature defined by $\frac{1}{n}\sum_{i=1}^{n} x_i$; $\bar{y}$ is the mean temperature defined by $\frac{1}{n}\sum_{i=1}^{n} y_i$; and n is the number of temperature data from 5 to 10 minutes (or 10 to 15 minutes/15 to 20 minutes in the event of large temperature differences from 5 to 10 minutes) after balloon release.

Figure 7 shows a histogram of the time offset to the elapsed time after the launch of RS2-91 radiosondes. The offset for most of the dual soundings was estimated to be within a range from -3 seconds to 2 seconds. After the time offset adjustment to the elapsed time after the launch of the RS2-91, the observation data (classified according to the time elapsed since balloon release) were analyzed.

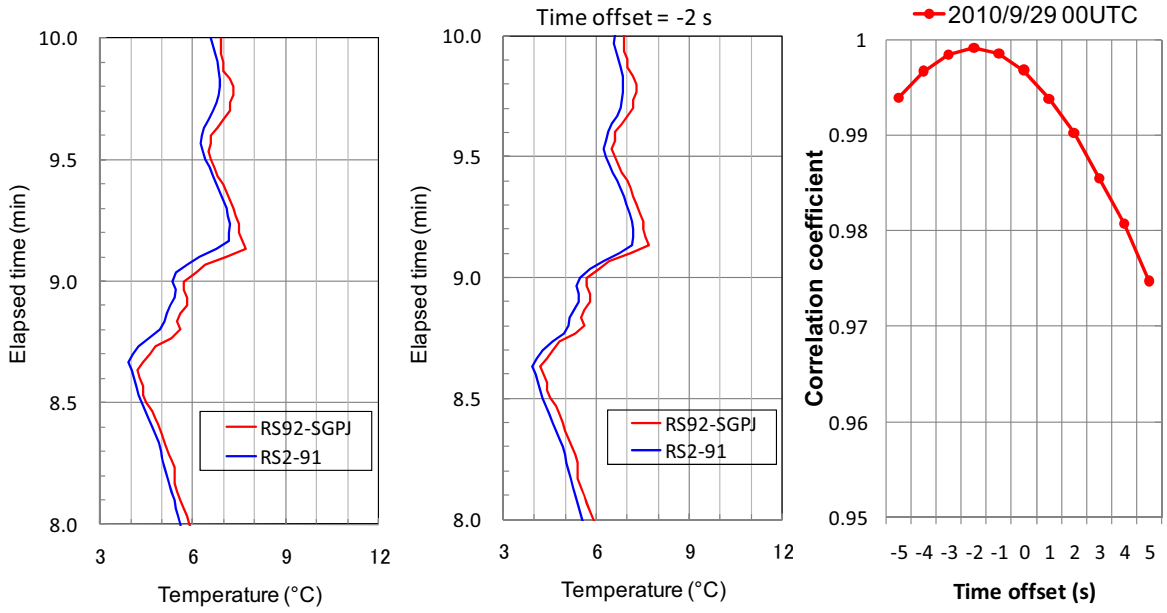

Figure 6. Example of the time adjustment procedure showing two time series of temperatures before (left) and after time offset adjustment (middle). The correlation coefficient between the two time series of temperatures shows a maximum value with a time adjustment of -2 seconds of the elapsed time for the RS2-91 radiosonde (right).

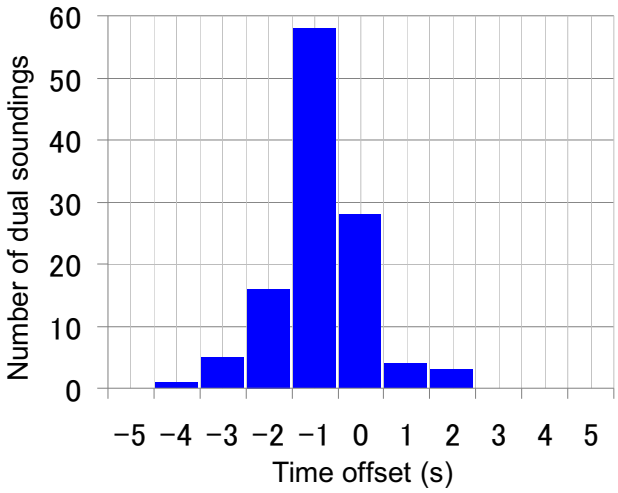

Figure 7. Histogram of time offset for the time elapsed since launch for RS2-91 radiosondes.

3.5 Rates of ascent of radiosondes

It is known that air temperature measurements are affected by radiosonde rates of ascent, the wake of the balloon, sensor specifications and solar/infrared radiation. Figure 8 shows box plots for the radiosonde rates of ascent during the four intensive observation periods (IOPs) of the field comparison. These rates were obtained from the RS92-SGPJ radiosondes every two seconds. It can be seen that the central 50% portions of the figures show values between 5 and 7 m/s in the troposphere, and between 5 and 8 m/s in the stratosphere. The rates of ascent in the range of 5 to 8 m/s were achieved to minimize ventilation and heating errors due to difference from the standard test conditions.

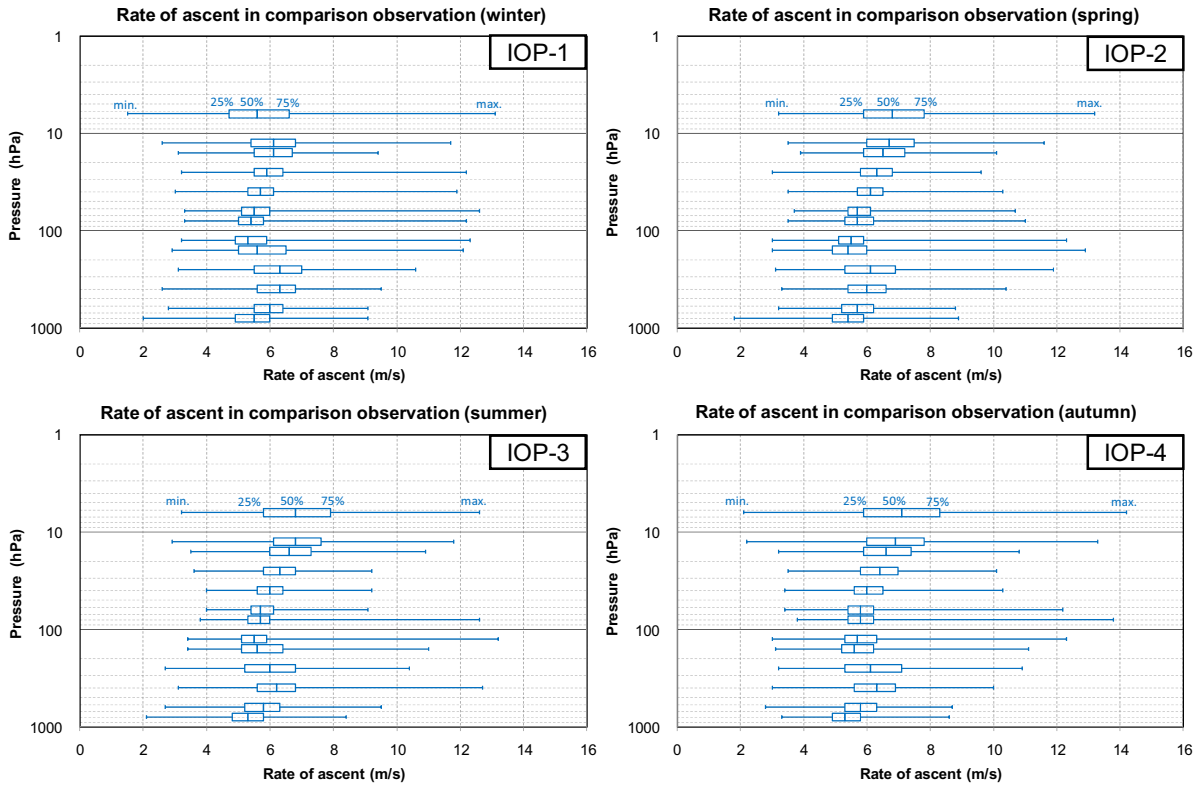

Figure 8. Box plots for radiosonde rates of ascent during the four intensive observation periods (IOPs) of the field comparison.

3.6 Radiosonde trajectories

Figures 9 a and b show plan views and vertical cross sections of radiosonde trajectories during the four intensive observation periods (IOPs) of the field comparison. The three-dimensional trajectories of the radiosondes were influenced by horizontal winds and the vertical velocities of the balloons. As radiosonde ascent took around 90 minutes, horizontal displacement was large in IOP-1 (winter), IOP-2 (spring) and IOP-4 (autumn), as Tateno is in a zone of prevailing westerly winds.

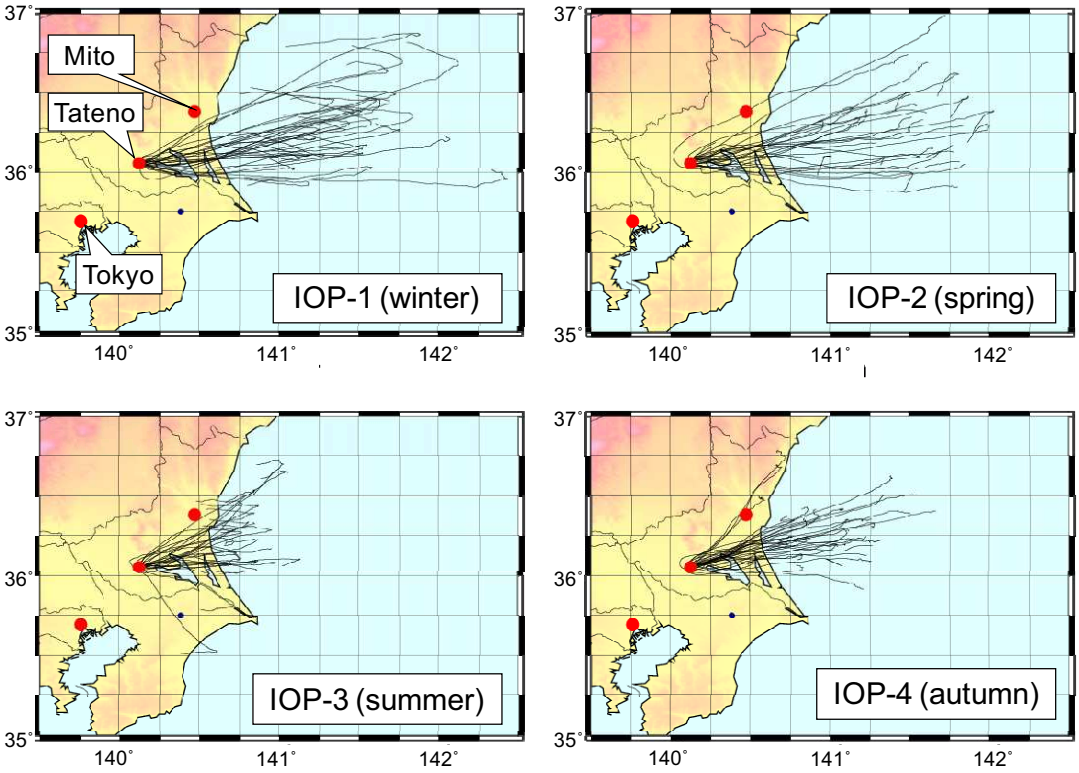

Figure 9 a. Plan views of the trajectories of radiosondes launched from Tateno during the four intensive observation periods (IOPs) of the field comparison. Locations of Tateno, Mito and Tokyo are shown by red closed circles.

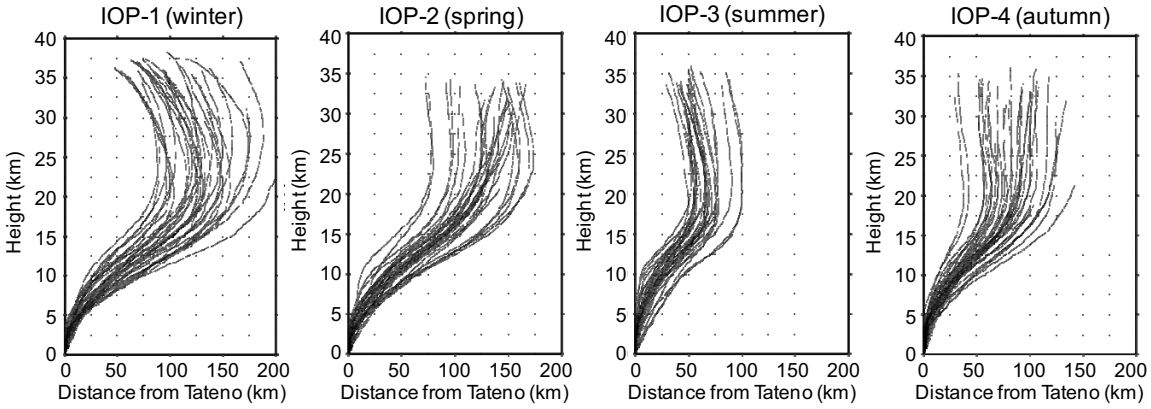

Figure 9 b. Vertical cross sections of the trajectories of radiosondes launched from Tateno during the four intensive observation periods (IOPs) of the field comparison.

3.7 Comparison at various elapsed times

The observational data were classified according to the time elapsed since balloon release, and were analyzed to elucidate the causes of differences between the two radiosondes. Comparison using elapsed times will provide radiosonde manufacturers and those involved in upper-air observations with useful information for improving radiosonde instruments and data processing procedures, as the radiosonde measurements were simultaneously obtained on the same balloon platform.

3.7.1 Pressure categories

For comparison using elapsed times, data obtained every two seconds on each flight were grouped into 13 categories according to the pressure values measured with the RS2-91, as shown in Table 4. The mean and the difference (RS92-SGPJ minus RS2-91) were calculated from the data obtained every two seconds in each pressure category for each flight. Data from different flights in the same pressure range were then gathered to create a dataset and obtain mean and difference profiles.

Table 4. Pressure categories for comparison using elapsed times

Category no.	Pressure range (hPa)	Category no.	Pressure range (hPa)	Category no.	Pressure range (hPa)
1	1,000 – 700	6	150 – 100	11	20 – 15
2	700 – 500	7	100 – 70	12	15 – 10
3	500 – 300	8	70 – 50	13	10 – 5
4	300 – 200	9	50 – 30		
5	200 – 150	10	30 – 20		

3.7.2 Number of dual soundings used to calculate mean and difference profiles

Table 5 shows the number of dual soundings used to calculate mean and difference profiles for pressure, temperature and relative humidity, and Table 6 shows the same for wind speed and wind direction. Several soundings with outliers were excluded when deriving the profiles.

Table 5. Number of dual soundings used to calculate mean and difference profiles for pressure, temperature and relative humidity.

IOP no.	Season	Period	Number of dual soundings		
			00 UTC (09 LST)	12 UTC (21 LST)	Total
1	Winter	3 Dec. 2009 to 15 Jan. 2010	13	12	25
2	Spring	1 Mar. 2010 to 19 Mar. 2010	14	14	28
3	Summer	24 May 2010 to 8 Jul. 2010	11	12	23
4	Autumn	27 Sep. 2010 to 26 Oct. 2010	14	13	27
1 – 4	–	–	**52**	**51**	**103**

Table 6. Number of dual soundings used to calculate mean and difference profiles for wind speed and wind direction.

IOP no.	Season	Period	Number of dual soundings		
			00 UTC (09 LST)	12 UTC (21 LST)	Total
1	Winter	3 Dec. 2009 to 15 Jan. 2010	14	15	29
2	Spring	1 Mar. 2010 to 19 Mar. 2010	15	15	30
3	Summer	24 May 2010 to 8 Jul. 2010	12	14	26
4	Autumn	27 Sep. 2010 to 5 Oct. 2010	6	5	11
1 – 4	–	–	**47**	**49**	**96**

3.7.3 Temperature

Figure 10 shows mean and difference (RS92-SGPJ minus RS2-91) profiles for temperature at 00 UTC (09 LST) and 12 UTC (21 LST) during the four IOPs. As the means of the differences for temperature at 00 UTC are shown to be statistically different from those

at 12 UTC based on the results of testing for differences between the two, the mean and difference profiles at 00 UTC and 12 UTC are indicated separately.

The results of the comparisons can be summarized as follows:

(1) The means of temperature differences between the RS92-SGPJ and the RS2-91 were less than 0.4°C both during the daytime (00 UTC) and at night (12 UTC) for all heights.
(2) The standard deviations of the temperature differences became larger in the stratosphere.
(3) The temperatures of the RS92-SGPJ were 0.4 – 0.2°C higher than those of the RS2-91 in the layer below 300 hPa at 00 UTC and in the layer above 30 hPa at 12 UTC.

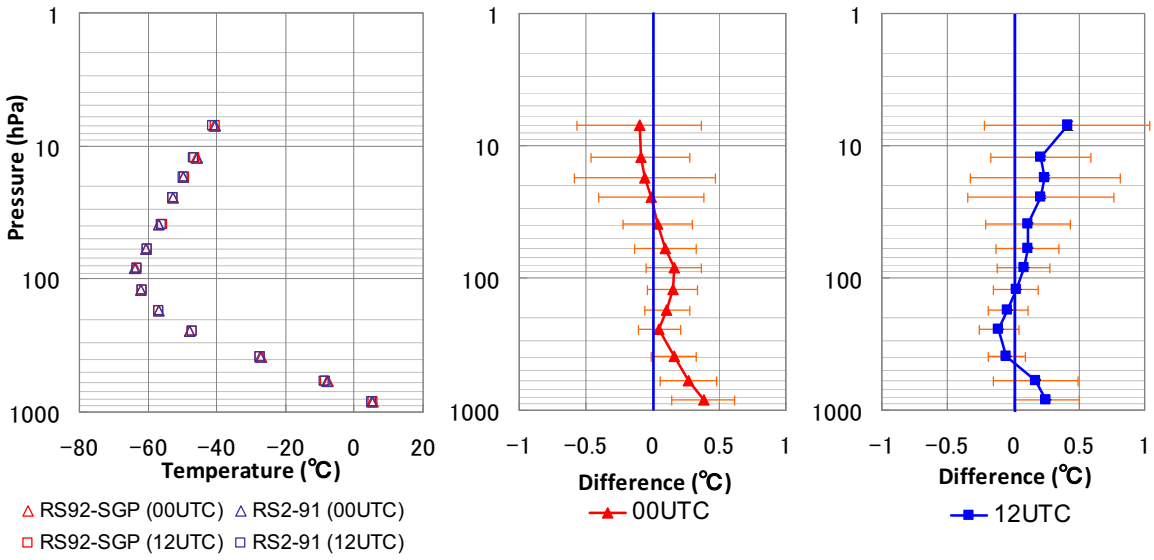

Figure 10. Mean and difference (RS92-SGPJ minus RS2-91) profiles for temperature. The error bars indicate the standard deviation.

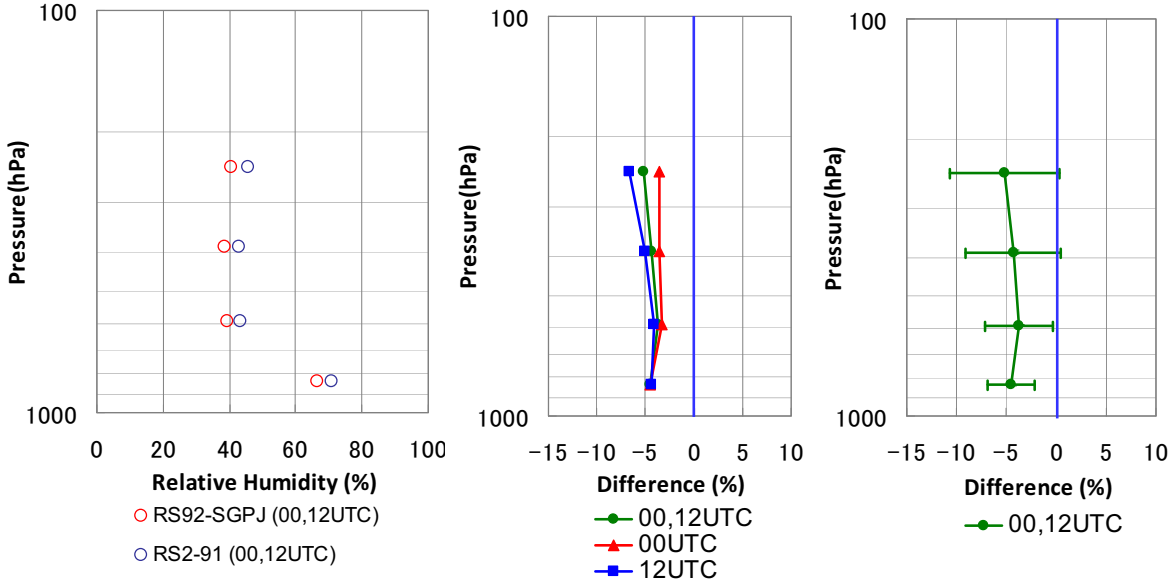

Figure 11. Mean and difference (RS92-SGPJ minus RS2-91) profiles for relative humidity. The error bars indicate the standard deviation.

3.7.4 Relative humidity

Figure 11 shows mean and difference (RS92-SGPJ minus RS2-91) profiles for relative humidity at 00 UTC (09 LST) and 12 UTC (21 LST). As the means of the differences for relative humidity at 00 UTC are shown not to be statistically different from those at 12 UTC based on the results of testing for differences between the two, the mean and difference profiles at 00 UTC and 12 UTC are merged. Figure 12a shows scatter plots of relative humidity of RS92-SGPJ to RS2-91 radiosondes, and Figure 12b shows scatter plots of relative humidity difference (RS92-SGPJ minus RS2-91) to relative humidity of RS2-91 radiosonde. Note that measurement of relative humidity below -40°C is not performed in Japan due to the low accuracy of humidity sensors.

The results of the comparisons can be summarized as follows:

(1) Relative humidity measured with the RS92-SGPJ was systematically lower than the RS2-91 by 4% – 5% on average.
(2) The standard deviations of relative humidity difference become larger as increasing altitude.
(3) Relative to the RS2-91, the RS92-SGPJ shows a dry bias which increases with relative humidity (Figures 12 a and b).

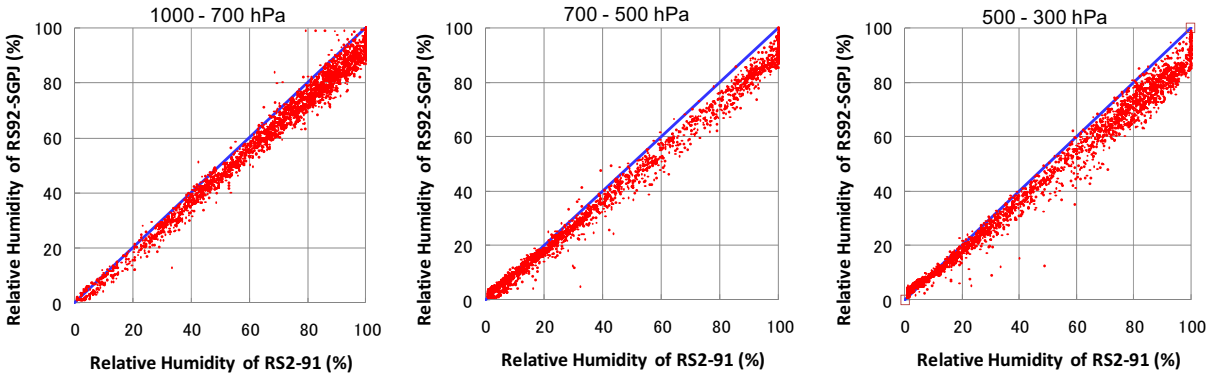

Figure 12a. Scatter plots of relative humidity of RS92-SGPJ to RS2-91 radiosondes. The humidity data was taken every 20 s during the dual soundings listed in Table 5.

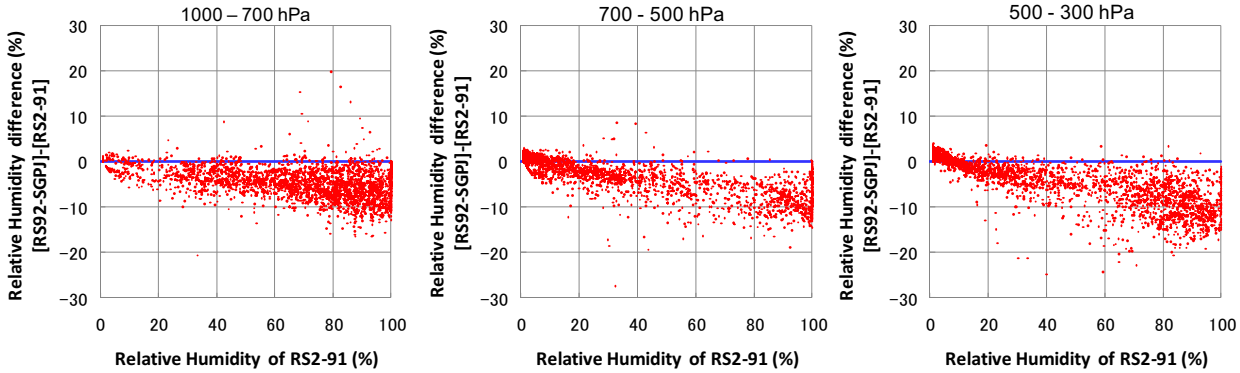

Figure 12b. Scatter plots of relative humidity difference (RS92-SGPJ minus RS2-91) to relative humidity of RS2-91 radiosonde. The humidity data was taken every 20 s during the dual soundings listed in Table 5.

3.7.5 Pressure and geopotential height

Figure 13 shows mean profiles for geopotential height and difference (RS92-SGPJ minus RS2-91) profiles for pressure and geopotential height. As the means of the differences for pressure and geopotential height at 00 UTC are shown not to be statistically different from those at 12 UTC based on the results of testing for differences between the two, the mean and difference profiles at 00 UTC and 12 UTC are merged.

The results of the comparisons can be summarized as follows:

(1) The RS92-SGPJ showed a general trend of larger pressure values than the RS2-91 both during the daytime and at night, from 0 near the surface to 0.6 hPa in the stratosphere.

(2) In the stratosphere, the height of the RS92-SGPJ became less than that of the RS2-91 as altitude increased, in accordance with the deviation of pressure described above.

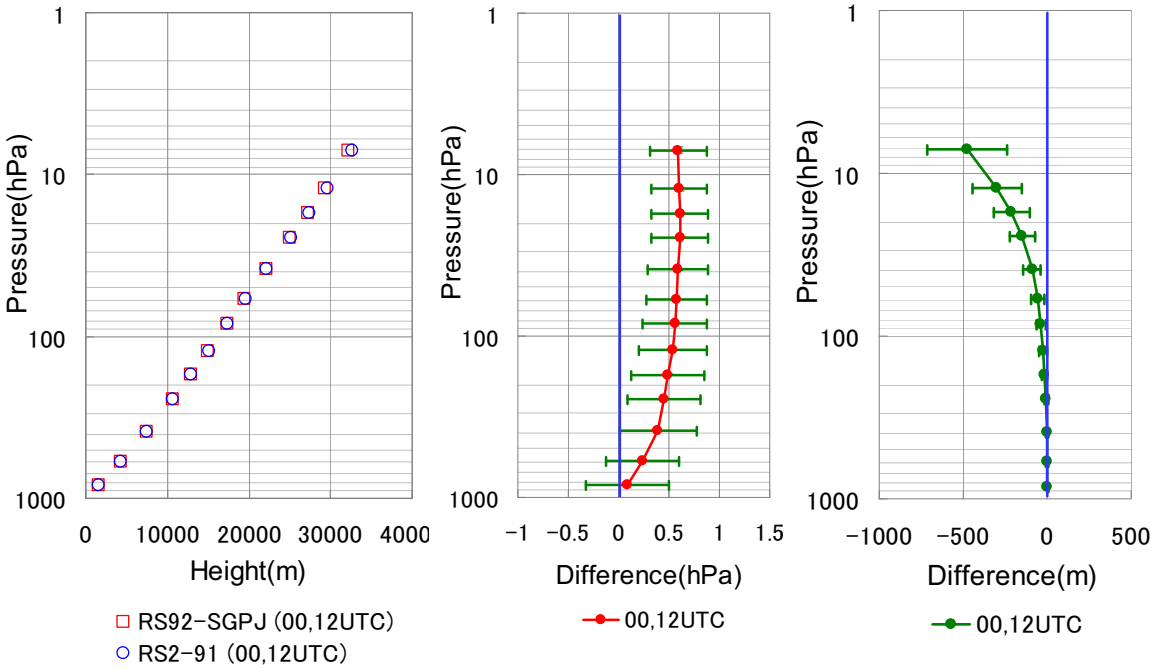

Figure 13. Mean profiles for geopotential height and difference (RS92-SGPJ minus RS2-91) profiles for pressure and geopotential height. The error bars indicate standard errors.

3.8 Comparison at different pressure levels

The comparison at pressure levels will be useful to users of radiosonde data, especially those involved in numerical weather prediction and climate continuity analyses.

Tables 8 -11 show the mean and differences (RS92-SGPJ minus RS2-91) at different pressure levels for temperature, relative humidity, geopotential height, wind speed and direction, and u (eastward) and v (northward) wind components, respectively. Since the mean of differences for temperature at 00 UTC are shown to be statistically different from those at 12 UTC based on the testing result for difference between two means, differences at 00 UTC and 12 UTC are indicated separately. The means of difference for other variables at 00 UTC and 12 UTC are shown not to be statistically different, so that mean and differences for the variables except temperature at 00 UTC and 12 UTC are merged. Note that measurement of relative humidity below -40°C is not performed in Japan due to low accuracy of humidity sensors.

The results of the comparisons can be summarized as follows:

(1) Temperature
- At all levels below 15 hPa, the means of temperature difference between RS92-SGPJ and RS2-91 are less than 0.4°C both in daytime (00 UTC) and in night (12 UTC).
- The standard deviations of temperature difference become larger than 0.5°C at all levels above 70 hPa.

(2) Relative humidity
- RS92-SGPJ showed 3 to 8% lower relative humidity values than RS2-91 at all pressure levels.

(3) Geopotential height

- In the stratosphere, the geopotential height of RS92-SGPJ becomes higher than the height of RS2-91. The difference of height between the radiosondes was 47.5 m at 5 hPa.

(4) Wind

- Good correspondence between RS92-SGPJ and RS2-91 radiosonde measurements of wind speed and direction, and u (eastward) and v (northward) wind components were found at all pressure levels during the IOPs.
- The differences of wind were less than 1.5 m/s in u (eastward) wind component and less than 1 m/s in v (northward) component.

Table 7. Means and differences (RS92-SGPJ minus RS2-91) at various pressure levels for temperature.

(a) 00 UTC (09 LST).

00 UTC					
Pressure level (hPa)	Mean temperature (℃)		Temperature difference [RS92-SGPJ]-[RS2-91] (℃)	Standard deviation of the temperature difference (℃)	Number of dual soundings
	RS92-SGPJ	RS2-91			
1000	11.74	11.68	**0.06**	0.28	49
925	8.90	8.60	**0.29**	0.28	52
900	8.01	7.71	**0.30**	0.22	52
850	6.06	5.68	**0.38**	0.43	52
800	3.72	3.31	**0.41**	0.59	52
700	-1.20	-1.47	**0.27**	0.27	52
600	-7.13	-7.33	**0.20**	0.24	52
500	-15.40	-15.59	**0.19**	0.29	52
400	-25.81	-25.90	**0.09**	0.24	52
350	-32.59	-32.56	**-0.03**	0.21	52
300	-39.88	-39.82	**-0.07**	0.25	52
250	-47.80	-47.68	**-0.12**	0.26	52
200	-54.26	-54.30	**0.04**	0.42	51
175	-56.52	-56.50	**-0.02**	0.38	51
150	-59.27	-59.31	**0.04**	0.37	51
125	-61.93	-61.89	**-0.04**	0.44	51
100	-64.50	-64.60	**0.10**	0.43	50
70	-62.24	-62.34	**0.10**	0.55	50
50	-59.06	-59.09	**0.03**	0.57	49
40	-57.15	-57.44	**0.29**	0.93	48
30	-54.55	-54.86	**0.32**	0.96	47
20	-50.70	-50.91	**0.21**	0.88	47
15	-48.45	-48.52	**0.08**	1.02	44
10	-42.66	-43.20	**0.53**	1.04	42
5	-32.28	-34.83	**2.55**	3.93	6

(b) 12 UTC (21 LST)

12 UTC					
Pressure level (hPa)	Mean temperature (℃)		Temperature difference [RS92-SGPJ]-[RS2-91] (℃)	Standard deviation of the temperature difference (℃)	Number of dual soundings
	RS92-SGPJ	RS2-91			
1000	12.54	12.36	**0.18**	0.21	47
925	9.45	9.27	**0.18**	0.22	51
900	8.25	8.06	**0.18**	0.20	51
850	5.58	5.38	**0.20**	0.27	51
800	3.07	2.87	**0.20**	0.36	51
700	-1.76	-1.96	**0.20**	0.35	51
600	-7.80	-7.87	**0.07**	0.19	51
500	-16.09	-16.10	**0.01**	0.34	51
400	-26.34	-26.21	**-0.13**	0.24	51
350	-32.53	-32.31	**-0.22**	0.21	51
300	-39.67	-39.43	**-0.24**	0.21	51
250	-46.73	-46.52	**-0.21**	0.29	51
200	-54.49	-54.27	**-0.22**	0.29	51
175	-57.03	-56.83	**-0.21**	0.34	51
150	-59.26	-59.18	**-0.08**	0.35	51
125	-61.48	-61.44	**-0.04**	0.41	51
100	-63.63	-63.59	**-0.04**	0.43	51
70	-62.08	-62.12	**0.04**	0.55	49
50	-57.93	-58.08	**0.14**	0.69	46
40	-56.19	-56.24	**0.05**	0.76	45
30	-53.92	-54.14	**0.22**	0.87	45
20	-50.82	-51.26	**0.44**	0.84	42
15	-48.07	-48.50	**0.42**	1.15	40
10	-42.39	-43.74	**1.35**	1.79	30
5	-34.46	-37.24	**2.79**	2.00	7

Table 8. Means and differences (RS92-SGPJ minus RS2-91) at various pressure levels for relative humidity.

00 UTC and 12 UTC					
Pressure level (hPa)	Mean humidity (%)		Humidity difference [RS92-SGPJ]-[RS2-91] (%)	Standard deviation of the humidity difference (%)	Number of dual soundings
	RS92-	RS2-91			
1000	72.9	77.1	**-4.2**	3.5	96
925	74.4	79.0	**-4.7**	3.1	101
900	74.2	78.5	**-4.3**	3.2	101
850	70.3	75.1	**-4.8**	3.6	101
800	65.4	70.0	**-4.6**	4.0	101
700	46.6	51.1	**-4.5**	3.8	102
600	38.5	42.1	**-3.5**	4.3	102
500	37.8	41.6	**-3.8**	4.9	103
400	38.4	43.5	**-5.1**	5.9	101
350	43.1	48.3	**-5.3**	5.3	84
300	43.7	49.6	**-6.0**	6.9	50
250	35.7	43.6	**-7.9**	7.0	9

Table 9. Means and differences (RS92-SGPJ minus RS2-91) at various pressure levels for geopotential height.

00 UTC and 12 UTC					
Pressure level (hPa)	Mean geopotential height (m)		Geopotential height difference [RS92-SGPJ]-[RS2-91] (m)	Standard deviation of the geopotential height difference (m)	Number of dual soundings
	RS92-SGPJ	RS2-91			
1000	127.0	127.2	**-0.2**	0.5	103
925	777.4	777.2	**0.3**	0.7	103
900	1004.4	1003.9	**0.6**	0.9	103
850	1475.0	1473.8	**1.1**	1.2	103
800	1969.4	1967.8	**1.6**	1.8	103
700	3043.4	3040.5	**2.9**	3.0	103
600	4257.6	4253.7	**3.9**	4.0	103
500	5655.5	5650.6	**4.9**	5.1	103
400	7304.2	7299.0	**5.2**	6.0	103
350	8257.8	8252.7	**5.1**	6.4	103
300	9327.3	9322.8	**4.5**	7.0	103
250	10552.7	10548.7	**4.0**	7.4	103
200	12000.2	11997.0	**3.2**	8.0	102
175	12850.7	12847.6	**3.0**	8.3	102
150	13821.6	13818.6	**3.0**	8.9	102
125	14956.0	14953.0	**3.0**	9.7	102
100	16331.8	16328.8	**3.1**	10.6	101
70	18519.0	18514.2	**4.7**	12.6	99
50	20618.6	20611.8	**6.8**	14.5	95
40	22027.3	22019.5	**7.9**	15.8	93
30	23858.8	23849.1	**9.7**	17.9	92
20	26473.7	26460.5	**13.2**	22.3	89
15	28357.5	28342.6	**14.9**	25.0	84
10	31062.4	31038.0	**24.4**	28.2	72
5	35641.0	35593.5	**47.5**	30.0	13

Table 10. Means and differences (RS92-SGPJ minus RS2-91) at various pressure levels for wind direction and speed.

00 UTC and 12 UTC					
Pressure level (hPa)	Mean wind direction (degree)		Wind direction difference [RS92-SGPJ]-[RS2-91] (degree)	Standard deviation of the wind direction difference (degree)	Number of dual soundings
	RS92-SGPJ	RS2-91			
1000	171.6	158.0	**0.8**	23.3	85
925	174.8	181.4	**1.8**	24.8	86
900	192.5	203.3	**1.9**	11.9	85
850	221.5	222.9	**-1.4**	24.0	83
800	232.9	245.1	**-3.3**	18.4	81
700	255.4	254.9	**0.5**	6.0	86
600	256.4	256.7	**-0.2**	3.9	89
500	258.1	259.1	**-0.9**	8.3	91
400	258.5	258.6	**-0.1**	2.1	89
350	258.0	258.3	**-0.3**	2.6	84
300	259.5	259.4	**0.1**	2.0	81
250	258.8	258.5	**0.3**	1.8	81
200	259.4	259.1	**0.3**	1.6	78
175	260.3	260.0	**0.3**	2.0	73
150	261.3	260.7	**0.6**	2.3	70
125	260.5	260.0	**0.5**	4.3	67
100	261.0	260.3	**0.6**	7.4	65
70	235.3	249.9	**2.0**	26.2	65
50	203.5	197.3	**0.7**	35.5	66
40	165.8	176.0	**-4.6**	35.8	65
30	152.5	148.6	**4.0**	31.8	67
20	128.9	130.5	**-1.6**	25.2	68
15	123.9	127.0	**-3.1**	19.7	65
10	115.9	121.2	**0.8**	19.1	59

00 UTC and 12 UTC					
Pressure level (hPa)	Mean wind velocity (m/s)		Wind velocity difference [RS92-SGPJ]-[RS2-91] (m/s)	Standard deviation of the wind velocity difference (m/s)	Number of dual soundings
	RS92-SGPJ	RS2-91			
1000	5.0	4.4	**0.6**	0.9	85
925	7.1	7.0	**0.1**	1.0	86
900	7.6	7.3	**0.2**	0.9	85
850	8.2	8.2	**0.0**	1.0	83
800	9.6	9.5	**0.1**	1.0	81
700	14.5	14.5	**0.0**	1.2	86
600	20.1	20.1	**0.0**	0.9	89
500	26.6	26.5	**0.2**	1.2	91
400	33.6	33.4	**0.2**	1.2	89
350	37.2	37.2	**0.1**	1.9	84
300	42.0	41.7	**0.3**	1.8	81
250	49.7	49.2	**0.5**	1.8	81
200	53.2	52.5	**0.7**	2.1	78
175	52.7	51.9	**0.8**	2.0	73
150	49.1	48.2	**0.9**	2.8	70
125	42.0	41.8	**0.2**	3.3	67
100	31.6	31.6	**0.1**	3.0	65
70	16.4	16.8	**-0.3**	3.4	65
50	10.1	8.8	**1.3**	3.1	66
40	8.4	7.2	**1.2**	2.6	65
30	7.2	6.5	**0.7**	2.6	67
20	8.8	8.0	**0.8**	2.5	68
15	10.5	9.5	**1.0**	2.2	65
10	15.8	14.2	**1.6**	3.1	59

Table 11. Means and differences (RS92-SGPJ minus RS2-91) at various pressure levels for u (eastward) and v (northward) wind components.

00 UTC and 12 UTC						00 UTC and 12 UTC					
Pressure level (hPa)	Mean U wind component (m/s)		U wind component difference [RS92-SGPJ]-[RS2-91] (m/s)	Standard deviation of the u wind component difference (m/s)	Number of dual soundings	Pressure level (hPa)	Mean v wind component (m/s)		V wind component difference [RS92-SGPJ]-[RS2-91] (m/s)	Standard deviation of the v wind component difference (m/s)	Number of dual soundings
	RS92-SGPJ	RS2-91					RS92-SGPJ	RS2-91			
1000	-0.9	-0.9	**0.0**	0.9	85	1000	-1.4	-1.2	**-0.2**	0.8	85
925	0.7	0.8	**-0.1**	1.1	86	925	0.0	0.0	**0.0**	1.0	86
900	1.8	1.9	**-0.1**	0.9	85	900	0.4	0.4	**0.1**	0.9	85
850	4.3	4.3	**0.0**	1.0	83	850	1.1	1.0	**0.1**	0.9	83
800	7.0	7.1	**0.0**	0.8	81	800	1.6	1.3	**0.3**	1.4	81
700	12.3	12.3	**0.0**	1.4	86	700	2.2	2.3	**-0.1**	1.7	86
600	18.4	18.4	**0.0**	0.9	89	600	3.7	3.7	**0.0**	0.8	89
500	24.4	24.3	**0.1**	1.2	91	500	5.5	5.4	**0.1**	0.9	91
400	31.1	31.0	**0.2**	1.3	89	400	7.0	7.0	**0.1**	1.0	89
350	34.7	34.6	**0.0**	1.9	84	350	7.6	7.4	**0.2**	1.6	84
300	39.4	39.1	**0.2**	1.7	81	300	7.9	8.0	**0.0**	1.5	81
250	46.6	46.2	**0.4**	1.8	81	250	9.8	9.9	**-0.1**	1.4	81
200	50.0	49.4	**0.7**	2.0	78	200	9.8	9.9	**-0.1**	1.5	78
175	50.1	49.3	**0.9**	2.0	73	175	9.3	9.6	**-0.3**	1.7	73
150	46.8	45.9	**0.8**	2.8	70	150	8.5	8.7	**-0.2**	1.8	70
125	40.0	39.9	**0.0**	3.2	67	125	7.3	7.8	**-0.4**	2.8	67
100	30.3	30.2	**0.1**	3.0	65	100	5.4	5.6	**-0.2**	3.1	65
70	14.7	15.5	**-0.8**	3.4	65	70	3.4	3.6	**-0.2**	2.7	65
50	5.4	6.0	**-0.6**	3.1	66	50	2.9	2.7	**0.2**	2.7	66
40	1.7	2.1	**-0.4**	3.0	65	40	0.7	1.5	**-0.8**	2.5	65
30	-1.8	-1.0	**-0.8**	2.7	67	30	0.7	1.2	**-0.5**	2.3	67
20	-5.3	-4.1	**-1.2**	2.2	68	20	0.8	1.1	**-0.4**	2.3	68
15	-6.6	-5.4	**-1.2**	2.3	65	15	0.6	0.9	**-0.3**	1.8	65
10	-9.8	-8.2	**-1.5**	3.0	59	10	-0.2	0.4	**-0.6**	2.7	59

4. Comparison of precipitable water vapor derived from GPS and radiosondes

Figure 14 shows the GPS antenna and data server installed at the Aerological Observatory to provide GPS-derived precipitable water vapor (GPS-PWV) measurements. The GPS receivers and antenna are the Trimble NetR8 GNSS reference receiver and TRM559800.00, respectively. The GPS-PWV value was derived from the GPS-PWV processing system including GPS-Inferred Positioning System and Orbit Analysis Simulation (GIPSY-OASIS II) software (Webb and Zumberge, 1993). More details of the derivation method are described by Shoji (2009).

The accuracy of GPS-PWV data has been shown to be comparable to that of radiosonde measurements. The root mean square difference between PW data derived from the GPS-PWV processing system and radiosonde observations is around 3.4 mm in summer and 1.6 mm in winter (Shoji et al., 2009). GPS-PWV data were derived every 5 minutes and used to complement the operational radiosonde replacement of the RS2-91 with the RS92-SGPJ in line with the need for independent measurements for moisture soundings.

Figure 15 shows a time series of PWV derived from GPS (the red line) and RS92-SGPJ radiosonde (the blue line) at Tateno from December 2009 to November 2010. The GPS-PWV data was averaged over 60 minutes after launch of radiosonde. Good correspondence between GPS-PWV and RS92-SGPJ radiosonde-derived precipitable water vapor is seen from December 2009 to November 2010.

Figure 16 shows a time series of PWV differences (RS92-SGPJ radiosonde-derived PWV minus GPS-PWV). The mean and standard deviation of PWV differences used for comparison are -0.65 mm and 1.30 mm, respectively. It should be noted that PWV data derived from the RS92-SGPJ were smaller by 0.65 mm on average than those of GPS-PWV.

Figure 14. GPS antenna (left) and data server (right) at the Aerological Observatory, Tateno.

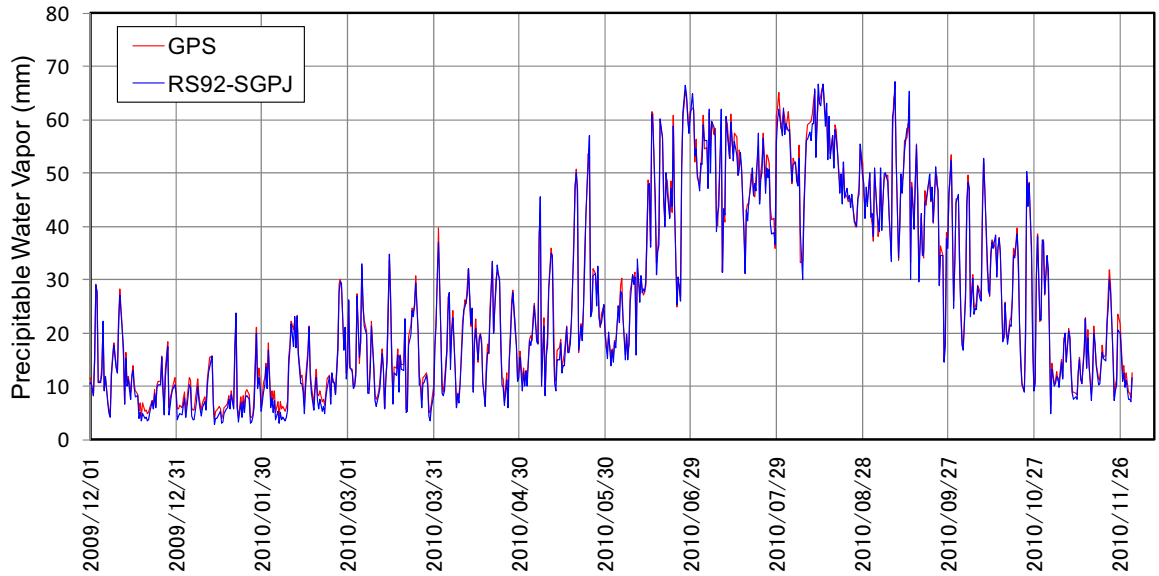

Figure 15. Time series of PWV derived from the GPS-PWV processing system (red line: —) and RS92-SGPJ radiosonde observations (blue line: —) at Tateno from December 2009 to October 2010. The GPS-PWV data was averaged for 60 minutes after launch of radiosonde.

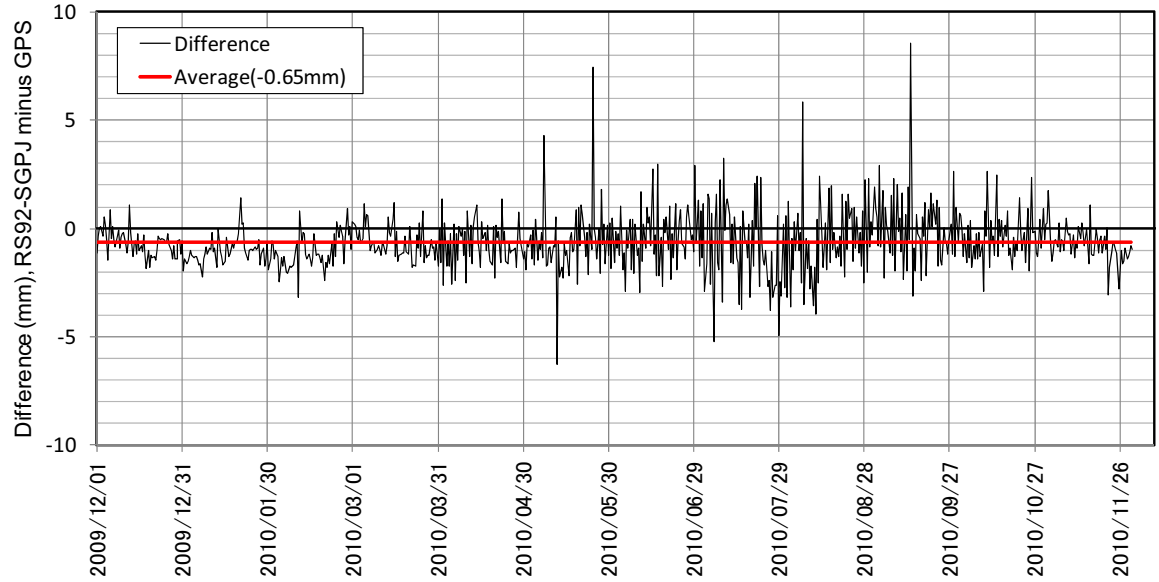

Figure 16. Time series of PWV differences (RS92-SGPJ radiosonde-derived PWV minus GPS-PWV) at Tateno from December 2009 to November 2010. The mean and standard deviation of PWV differences are -0.65 mm and 1.30 mm, respectively. Number of data used for comparison is 730. The red line shows the mean PWV difference (-0.65 mm).

Figure 17 and Table 12 show scatter plots and statistics for precipitable water vapor (PWV) derived from GPS and two radiosondes (radiosonde minus GPS), PWV difference (radiosonde-PWV minus GPS-PWV) and relative PWV difference (PWV difference divided by the GPS-PW) during four intensive observation periods (IOPs), respectively. These have shown a good agreement between GPS-PWV and two radiosonde-derived PWVs.

It is indicated that the RS92-SGPJ radiosonde-derived PWV was smaller by 0.53 mm on average than GPS-PWV and that the RS2-91 radiosonde-derived PWV was larger by 0.52 mm on average than GPS-PWV. It should be noted that the relative PWV difference of the RS92-SGPJ and the RS2-91 were -4.3% and 0.3%, respectively. These results are in agreement with the dry bias of the RS92-SGPJ relative humidity to the RS2-91 shown in Figure 11 and with the PWV differences (RS92-SGPJ radiosonde-derived PWV minus GPS-PWV) from December 2009 to November 2010 shown in Figure 16.

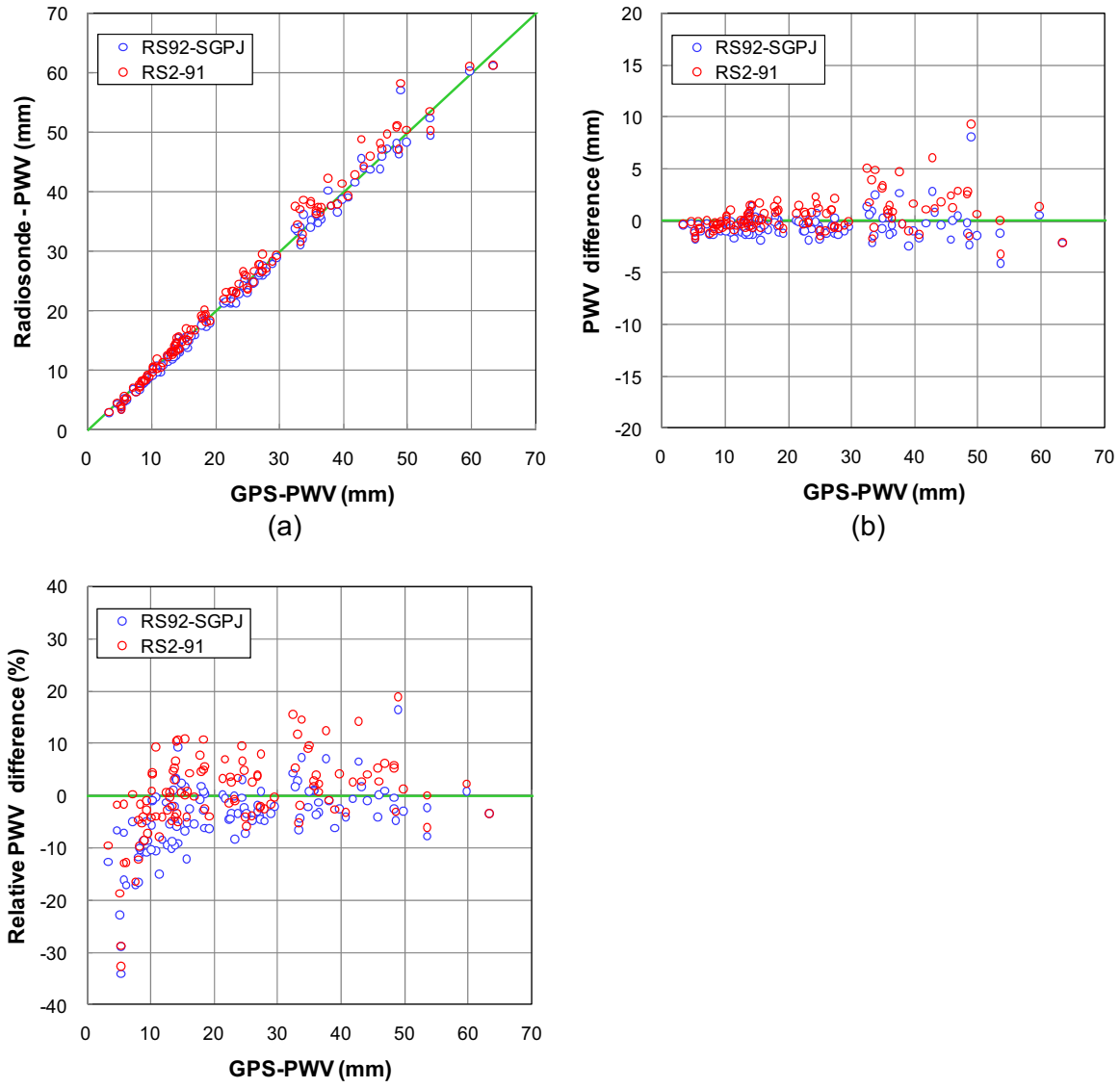

Figure 17. Scatter plots of GPS-PWV to (a) radiosonde-PWV, (b) PWV difference (radiosonde minus GPS) and (c) relative PWV difference defined as the PWV difference divided by the GPS-PW. Number of data used for comparison is 114 during four intensive observation periods (IOPs).

Table 12. Mean and standard deviation (Std dev) for precipitable water vapor (PWV) derived from GPS and two radiosondes, PWV difference (radiosonde minus GPS) and relative PWV difference defined as the PWV difference divided by the GPS-PW. Number of data used for comparison is 114 during four intensive observation periods (IOPs).

Statistics	Precipitable water vapor (mm)			PWV difference (mm)		Relative PWV difference (%)	
	GPS derived	RS92-SGPJ derived	RS2-91 derived	RS92-SGPJ	RS2-91	RS92-SGPJ	RS2-91
Mean	**23.46**	**22.93**	**23.98**	**-0.53**	**0.52**	**-4.3**	**0.3**
Std dev	14.20	14.41	14.92	1.28	1.72	6.8	7.7

5. Comparison of winds derived from Doppler lidar and radiosondes

Figure 18 shows the Doppler lidar instrument (Mitsubishi Electric Corporation, LR-09F III S) installed at the Aerological Observatory to provide Doppler lidar-derived wind data as independent measurements for wind soundings. The instrument measures the passing speed of aerosols (which is equivalent to the wind velocity) by detecting pulsed laser beam

light scattered by them. The unit's height range, resolution and observation cycle were 1,500 m, 75 m and 7.2 s, respectively. Winds were measured according to the measurement principle of a conical VAD scan with an elevation angle of 80 degrees over 72 s. The specifications of the Doppler lidar are summarized in Table 13.

Figure 19 shows a comparison of the u (eastward) and v (northward) component mean and difference profiles between Doppler lidar and the RS92-SGPJ radiosonde launched from Tateno at 1130 UTC on 29 September 2010. Both profiles show excellent correspondence.

Table 14 shows a statistical comparison of horizontal wind velocity (VEL), direction (DIR), u (eastward) wind component (U) and v (northward) component (V) between Doppler lidar and RS92-SGPJ radiosonde at Tateno during the period from December 2009 to November 2010. The overall bias of horizontal wind velocity and direction are 0.4 m/s and 1.9 °, and standard deviation of difference 1.1 m/s and 29.1 °, respectively. These have shown a good agreement between the Doppler lidar and radiosonde data.

Figure 18. Doppler lidar at the Aerological Observatory, Tateno.
(Mitsubishi Electric Corporation, LR-09F III S)

Table 13. Doppler lidar specifications (Mitsubishi Electric Corporation, LR-09F III S).

Wavelength	1.5 – 1.6 μ m
Observation mode	Conical scanning (elevation angle: 80 deg)
Pulse length	200 ns, 500 ns*, 1,000 ns (*: operational mode)
Range resolution	30 m, 75 m*, 150 m (*: operational mode)
Range	30 – 600 m, 75 – 1,500 m*, 150 – 3,000 m (*: operational mode)
Number of range gate	20
Observation velocity	-30 – 30 m/s
Observation data	Wind (u, v, w)

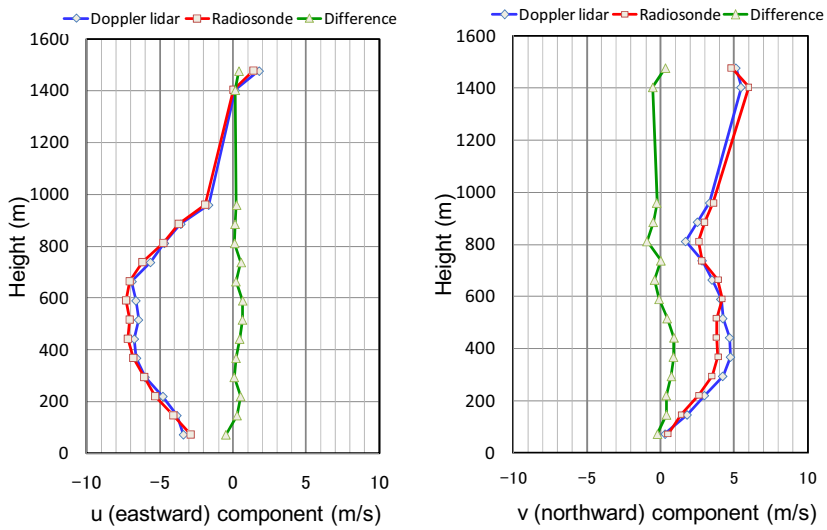

Figure 19. Comparison of u (eastward) and v (northward) component mean and difference profiles between Doppler lidar and the RS92-SGPJ radiosonde in Tateno at 1130 UTC (2030 LST) on 29 September, 2010.

Table14. Statistical comparison of horizontal wind velocity (VEL), direction (DIR), u (eastward) wind component (U) and v (northward) component (V) between Doppler lidar and the RS92-SGPJ radiosonde at Tateno during the period from December 2009 to November 2010. Systematic bias (Bias, Doppler lidar minus RS92-SGPJ) and standard deviation (Std dev) are shown.

Height (m AGL)	Number of Soundings	VEL (m/s)		DIR (°)		U (m/s)		V (m/s)	
		Bias	Std dev	Bias	Std dev	Bias	Std dev	Bias	Std dev
all	**4448**	**0.4**	1.1	**1.9**	29.1	**0.1**	1.0	**0.0**	1.1
74	424	**0.8**	1.1	**-0.6**	35.5	**0.0**	1.1	**0.1**	1.1
148	437	**0.4**	1.0	**2.2**	33.2	**0.0**	1.0	**0.0**	1.1
221	442	**0.5**	0.9	**1.1**	34.6	**0.1**	1.1	**0.1**	1.1
295	429	**0.4**	1.0	**1.8**	29.4	**0.1**	1.0	**0.1**	1.0
369	404	**0.4**	1.0	**4.9**	27.3	**0.1**	1.0	**0.0**	1.0
443	377	**0.4**	1.0	**3.5**	25.1	**0.1**	1.0	**0.1**	1.0
517	355	**0.4**	1.1	**0.3**	23.0	**0.1**	1.0	**0.1**	1.1
591	307	**0.3**	1.0	**3.3**	17.7	**0.2**	0.9	**0.1**	1.1
664	280	**0.2**	1.1	**1.9**	23.9	**0.2**	1.1	**0.0**	1.1
738	226	**0.2**	1.1	**-0.8**	22.6	**0.1**	1.0	**-0.1**	1.5
812	199	**0.4**	1.3	**-1.2**	26.5	**0.1**	1.2	**0.0**	1.1
886	154	**0.3**	1.3	**1.3**	29.9	**0.0**	1.1	**0.0**	1.1
960	126	**0.5**	1.2	**7.3**	28.7	**0.0**	1.1	**0.1**	1.1
1034	82	**0.4**	1.0	**9.5**	34.9	**0.2**	0.9	**0.0**	1.1
1107	69	**0.6**	1.3	**-4.8**	39.0	**0.3**	1.2	**0.2**	1.0
1181	53	**1.0**	2.6	**-2.6**	33.8	**0.1**	1.3	**-0.2**	1.5
1255	31	**0.1**	0.8	**3.2**	30.7	**0.1**	1.3	**-0.3**	0.8
1329	23	**0.5**	0.9	**5.1**	39.4	**0.3**	1.2	**0.0**	0.9
1403	17	**0.5**	1.3	**6.4**	19.7	**-0.2**	1.3	**0.2**	1.4
1476	13	**0.6**	1.5	**24.1**	49.0	**0.0**	0.6	**0.3**	1.1

6. Upper-air temperature trends for 1956–2010

Figure 20 shows upper-air temperature trends during 1956–2010 at Tateno for selected pressure levels using monthly uncorrected (blue lines) and corrected (red lined) temperature at 12 UTC. The temperature corrections of systematic biases due to radiosonde instrument changes (RSII-56, RS2-80, RS2-91 and RS92-SGPJ) at Tateno since 1956 are applied to drive the upper-air temperature trends. A positive temperature trend of 0.1-0.2 °C/10 year in the troposphere and a negative trend up to -0.4 °C/10 year in the stratosphere are remarkable. These corrections will provide more accurate temperature trends for climatic studies.

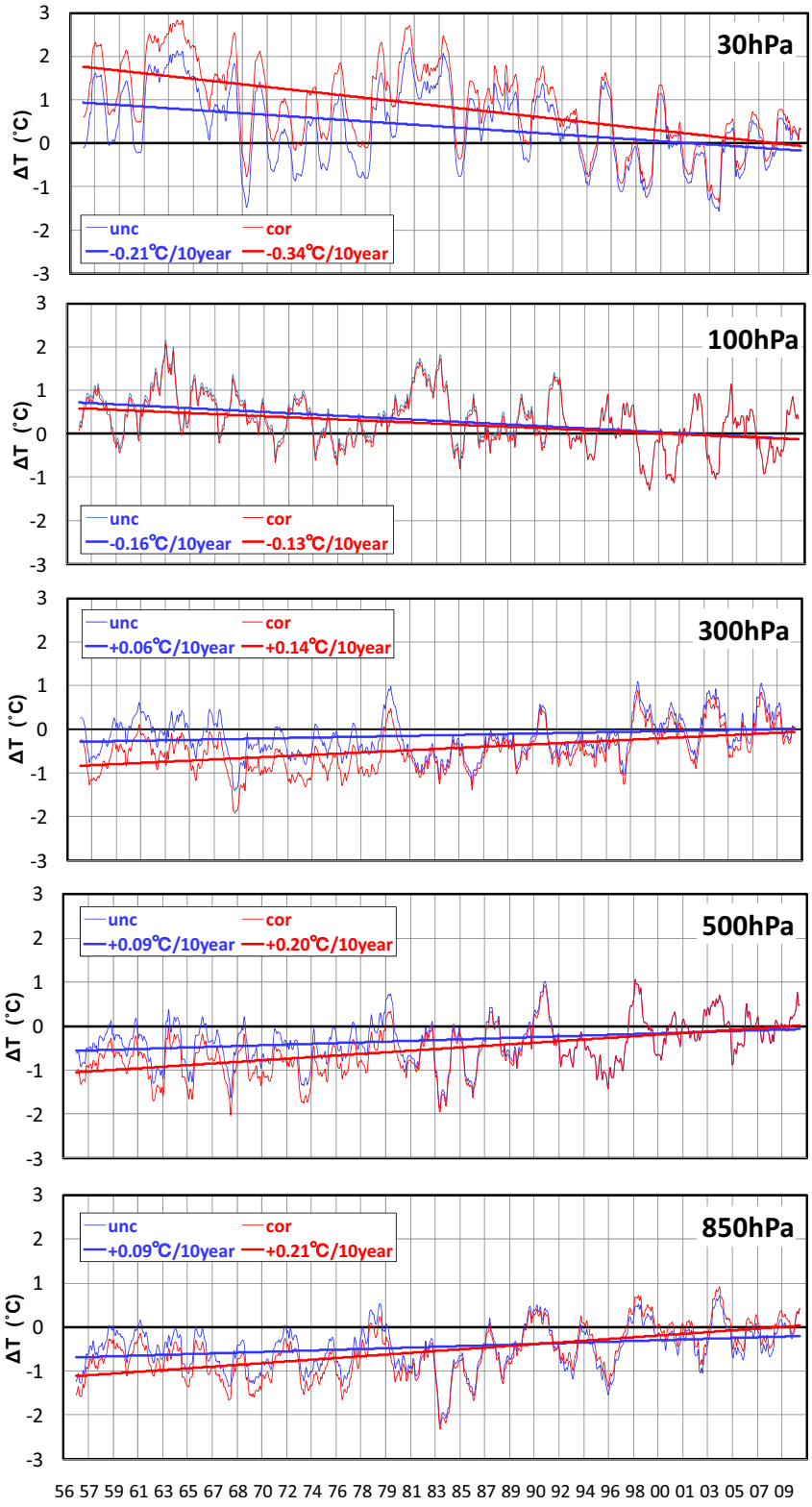

Figure 20. Upper-air temperature trends during 1956–2010 at Tateno for selected pressure levels using monthly uncorrected (blue lines) and corrected (red lined) temperature at 12 UTC. The temperature corrections of systematic biases due to radiosonde instrument changes (RSII-56, RS2-80, RS2-91 and RS92-SGPJ) at Tateno since 1956 are obtained by field comparisons for radiosonde replacements. ΔT (°C): 12-month moving average of monthly temperature anomaly from 2001-2010 average.

PART II SPATIAL VARIABILITY OF GPS-PWV

1. Introduction

JMA has started to monitor the distribution of GPS derived precipitable water vapour (GPS-PWV) over the Japanese Islands in near real time since May 2008. The GPS-PWV is obtained using data from the GEONET (GPS Earth Observation Network) system operated by the Geospatial Information Authority of Japan (GSI). In GEONET, about 1,200 GPS receivers are located throughout Japan to observe crustal deformation with a mean distance of 15 to 25 km.

The GPS-PWV was derived from the GPS-PWV processing system including GPS-Inferred Positioning System and Orbit Analysis Simulation (GIPSY-OASIS II) software (Webb and Zumberge, 1993). The root mean square difference between PW data derived from the GPS-PWV processing system and that from upper sounding is around 3.4 mm in summer and 1.6 mm in winter (Shoji, 2009). More details of the derivation method are described by Shoji (2009).

GPS-PWV data derived from a dense GPS network in Japan was used to examine the spatial variability for precipitable water vapour to discuss collocation issue of observation.

2. Methodology

To clarify collocation measurements of precipitable water vapour, spatial variability of GPS-PWV was analyzed by comparing the GPS-PWV at Tateno with those from 75 stations within distance of 100 km from Tateno. The GPS-PWV value was derived every 5 minutes from the GPS-PWV processing system (Shoji, 2009). Using the average 30 min GPS-PWV values from every 5 min value, the spatial variability of GPS-PWV was analyzed.

The spatial variability of GPS-PWV was described by the following statistical measures:

(1) GPS-PWV monthly means and differences from Tateno.
(2) Correlation coefficients between GPS-PWV at Tateno and those at other stations.
(3) Standard deviations of residuals defined as differences between observational values and predicted values from a linear regression with GPS-PWV at Tateno (the explanatory variable) and those at other stations (the dependent variable).

GPS-PWV monthly mean ($\overline{X_i}$) and difference (ΔX_i) from Tateno are calculated from Equation (2) and (3), respectively.

$$\overline{X_i} = \frac{1}{N}\sum_{j=1}^{N} X_{ij} \tag{2}$$

$$\Delta X_i = \overline{X_i} - \overline{X_0} \tag{3}$$

where X_{ij} : the GPS-PWV at the station (i), in time of the observations (j), N : number of GPS-PWV data in month, and $\overline{X_0}$: GPS-PWV monthly mean at Tateno.

Correlation coefficient (r_i) between GPS-PWV at Tateno and those at other station (i) is calculated from Equation (4).

$$r_i = \frac{\sum_{j=1}^{N}(X_{ij} - \overline{X_i})(X_{0j} - \overline{X_0})}{\sqrt{\sum_{j=1}^{N}(X_{ij} - \overline{X_i})^2}\sqrt{\sum_{j=1}^{N}(X_{0j} - \overline{X_0})^2}} \tag{4}$$

The high correlation is expected under the condition of a uniform and steady GPS-PWV field.

Equation (5) gives the standard deviation of residuals (SR_i) defined as differences between observational values and predicted values from a linear regression with GPS-PWV at Tateno (the explanatory variable) and those at other stations (the dependent variable).

$$SR_i = SD_i\sqrt{1-r_i^2} \quad (5)$$

where SD_i : standard deviation of X_{ij} . Since variations of the GPS-PWV at Tateno could not explain all variations of GPS-PWV values at other station, the standard deviation of residuals is a measure of errors that could not be expressed by GPS-PWV at Tateno.

3. Results

3.1 GPS-PWV monthly mean and differences from Tateno

Figure 21 shows GPS-PWV monthly mean and differences from Tateno in January 2010, April 2010, July 2010 and October 2010. As shown in Figure 15, GPW-PWV varied from month to month over a wide range (about 8 mm in January 2010 to more than 50 mm in July 2010). It is also noted from the GPS-PWV differences fields that there was a small increase along a gradient northwest to southeast in December 2009, north to south in April 2010, southeast to northwest in July 2010 and north to south in October 2010. A remarkable annual cycle in GPS-PWV and a small gradient from month to month in GPS-PWV differences are noted.

3.2 Correlation coefficient of GPS-PWV

Figure 22 shows monthly correlation coefficients between GPS-PWV at Tateno and those at other stations as a function of distance from Tateno. It is noted that the correlation between GPS-PWV at Tateno and those at other stations showed a decreasing function of distance from Tateno, and that there was a high correlation coefficient more than 0.85 within the distance of 80 km from Tateno in all month. In July through September 2010 correlation coefficients became decreasing below 0.85 over the distance of 80 km from Tateno. Since the high correlation means that the GPS-PWV variations at Tateno explain most of GPS-PWV variations at other station, the high correlation is a measure of representativeness.

3.3 Standard deviation of GPS-PWV residuals

Figure 23 shows monthly standard deviations of GPS-PWV residuals given by Equation (5) as a function of distance from Tateno. It is noted that the standard deviation of GPS-PWV residuals showed an increasing function of distance from Tateno. The standard deviation of residuals became larger as increasing distance from Tateno. Furthermore the standard deviations of residuals were larger than 4 mm in June through September within distance of 100 km from Tateno.

Since the standard deviation of residuals is a measure of errors which are not explained by a linear regression, the area less than a specific standard deviation of residuals indicates representative area. For a specific standard deviation of residuals of 3 mm, representative area became wider area in cold season months than in summer season.

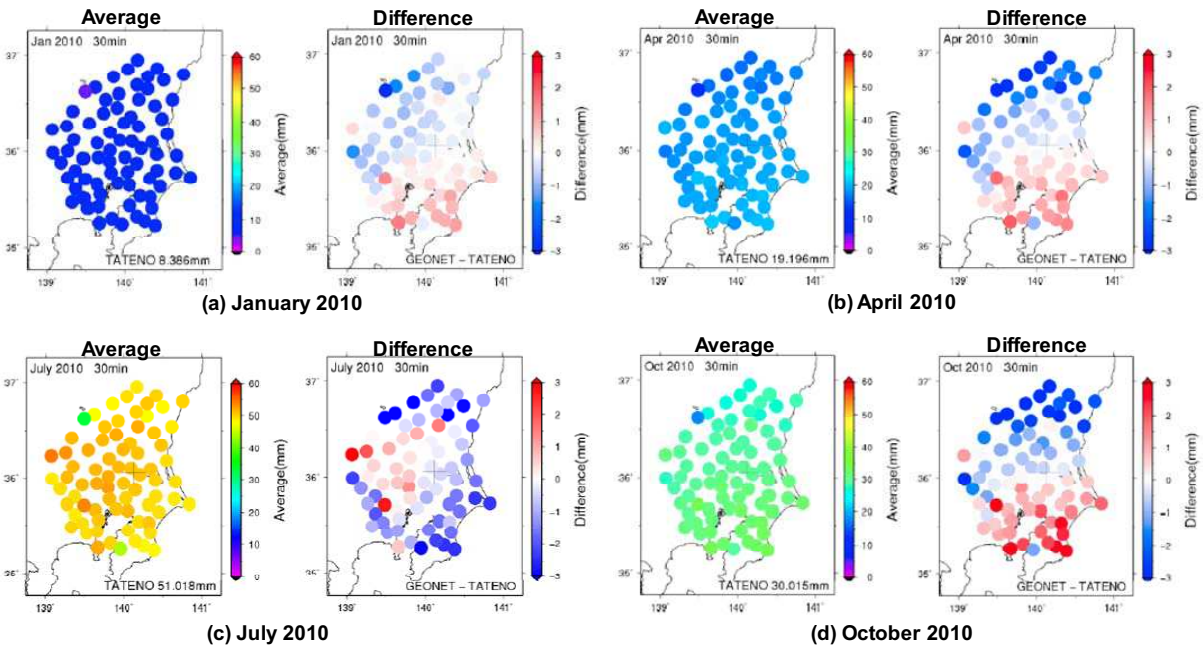

Figure 21. GPS-PWV monthly mean and differences from Tateno in (a) January 2010, (b) April 2010, (c) July 2010 and (d) October 2010.

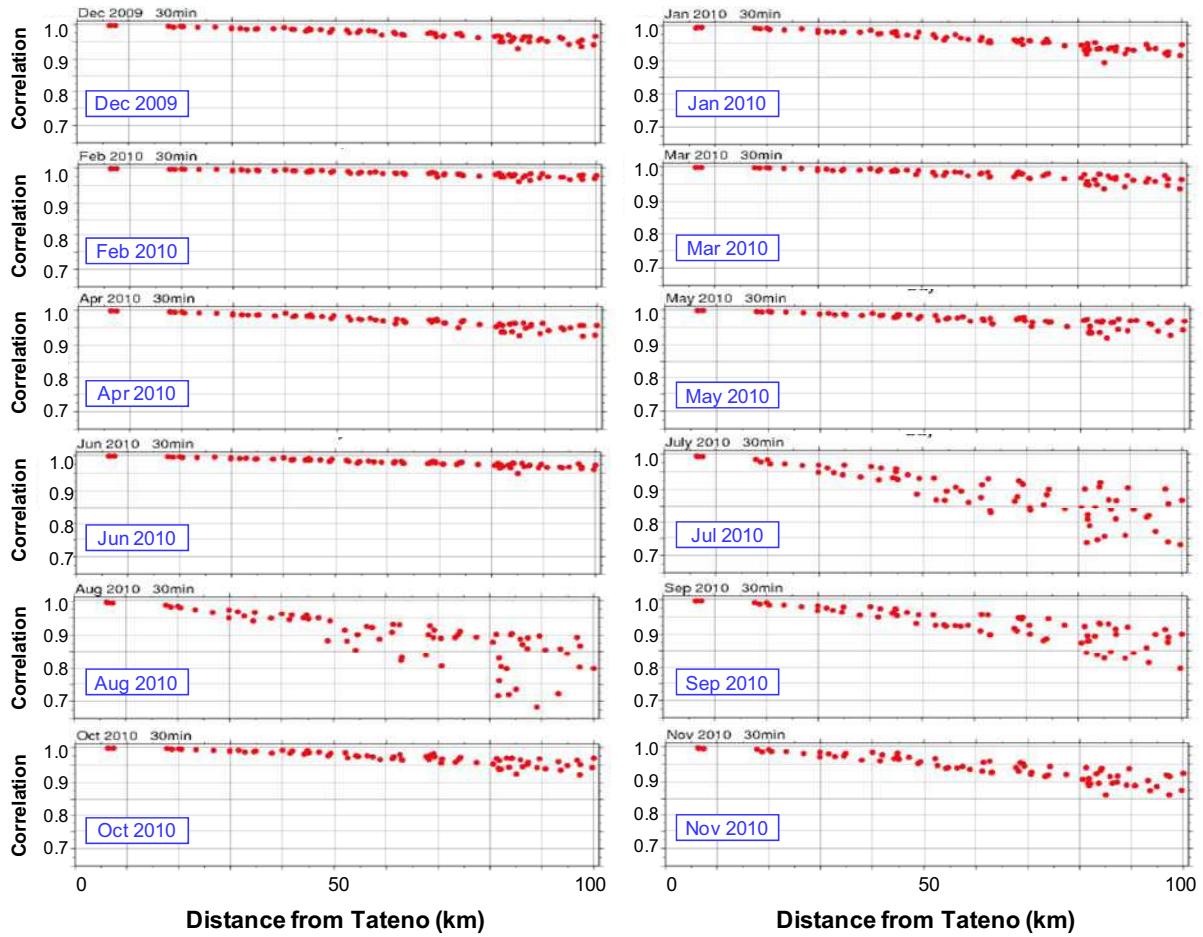

Figure 22. Correlation coefficient between GPS-PWV at Tateno and those at other stations as a function of distance from Tateno.

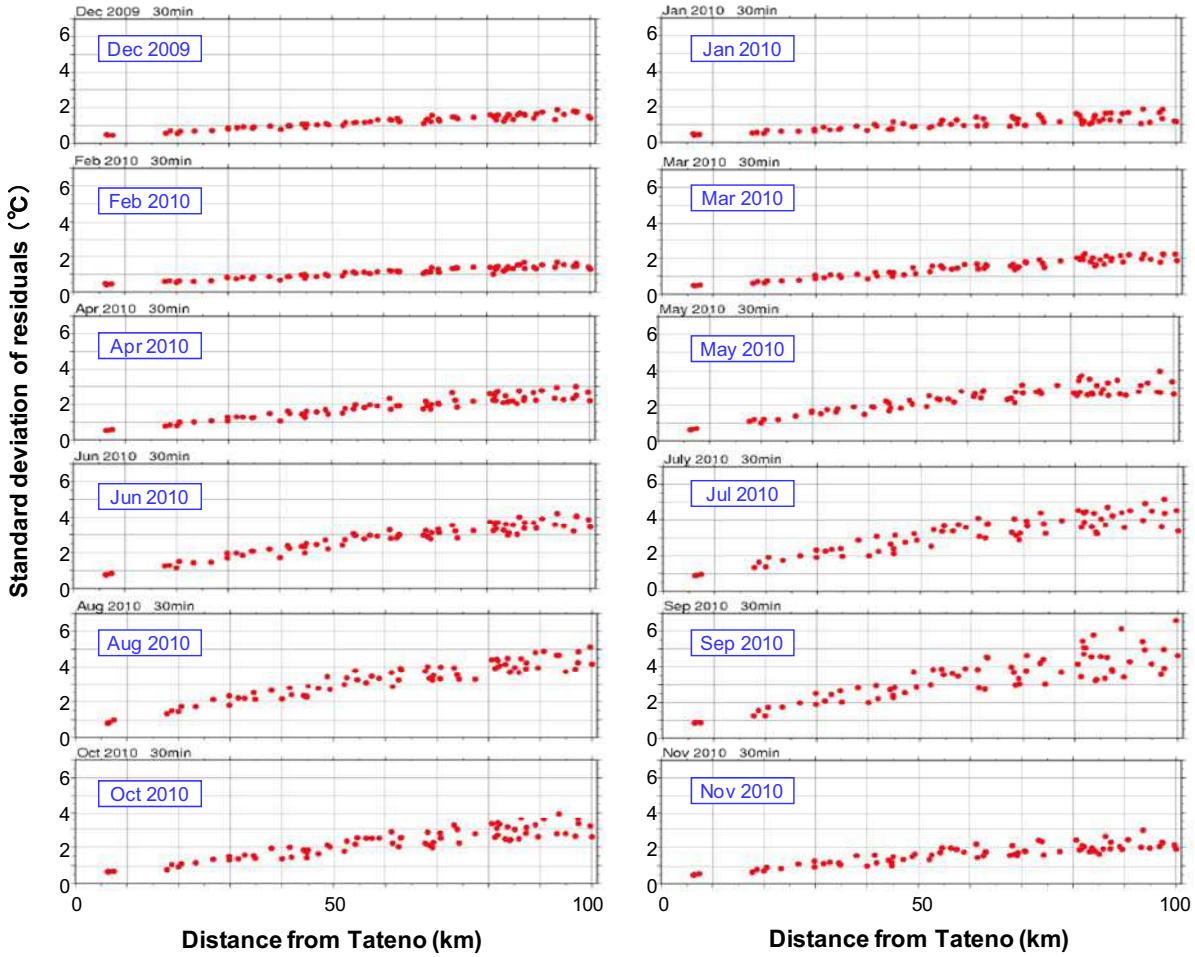

Figure 23. Standard deviation of GPS-PWV residuals as a function of distance from Tateno. The GPS-PWV residuals are defined as differences between observational values and predicted values from a linear regression with GPS-PWV at Tateno (the explanatory variable) and those at other stations (the dependent variable).

Acknowledgements

GEONET data was provided by the Geospatial Information Authority of Japan (GSI). We are grateful to the members of the Geospatial Information Authority of Japan (GSI).

References

da Silveira, R., G. Fisch, L. Machado, A. Dall'Antonia, L. Sapucci, D. Fernandes, and R. Marques, 2006: WMO intercomparison of GPS radiosondes, Alcantara, Brazil, 2001. WMO/TD No. 1314, Instruments and Observing Methods Report No. 90, World Meteorological Organization, Geneva, 65 pp. [available online at http://www.wmo.int/pages/prog/www/IMOP/publications/IOM-90_RSO-Brazil/IOM-90_RSO_EMA_Alcantara2001.pdf]

JMA, 2004: Manual guide of upper-air observation (in Japanese), Japan Meteorological Agency, App. 10 - App. 17.

Meisei Electric Co., Ltd., 2010: Product guide - RS2-91 type radiosonde (in Japanese), [Available online at http://www.meisei.co.jp/products/meteo/rs291.html.]

Nash, J., R. Smout, T. Oakley, B. Pathack, S. Kurnosenko, 2006: WMO Intercomparison of High Quality Radiosonde Systems. Vacaos, Mauritius, 2005. WMO/TD No. 1303, Instrument and Observing Methods Report, No. 83, World Meteorological Organization, Geneva, 118 pp.

Peterson, T.C., and I. Durre, 2004: A climate continuity strategy for the radiosonde replacement system transition. 8th AMS Symposium on Integrated Observing and

Assimilation Systems for Atmosphere, Oceans, and Land Surface, Seattle, WA, Jan. 10–15, 2004.

Shoji Y., 2009: A study of near real-time water vapor analysis using a nationwide dense GPS network of Japan, *J. Meteor. Soc. Japan*, **87**, 1 – 18.

Vaisala Oyj, 2005: Revised Solar Radiation Correction Table RSN2005 for Temperature Sensor, [Available online at http://www.vaisala.com/en/products/soundingsystemsandradiosondes/soundingdatacontinuity/Pages/solarradiationcorrectiontable.aspx]

Vaisala Oyj, 2010: Vaisala Radiosonde RS92-SGP, [available online at http://www.vaisala.com/Vaisala%20Documents/Brochures%20and%20Datasheets/RS92SGP-Datasheet-B210358EN-E-LoRes.pdf]

Yagi, S., A. Mita, and N. Inoue, 1996: WMO international radiosonde intercomparison phase IV (Tsukuba, Japan, 1993) final report. WMO/TD No. 742, Instruments and Observing Methods Report, No. 59, World Meteorological Organization, Geneva, 130 pp.

World Meteorological Organization, 2003: Manual on the Global Observing System. Volume I (Annex V to the WMO Technical Regulations), Global Aspects, WMO‑No. 544, Geneva.

Webb, F. H., and J. F. Zumberge, 1993: An introduction to the GIPSY/OASIS-II, JPL Publ., D-11088.